



Implications for Extraterrestrial Hydrocarbon Chemistry: Analysis of Acetylene (C_2H_2) and D2-acetylene (C_2D_2) Ices Exposed to Ionizing Radiation via Ultraviolet–Visible Spectroscopy, Infrared Spectroscopy, and Reflectron Time-of-flight Mass Spectrometry

Matthew J. Abplanalp^{1,2} and Ralf I. Kaiser^{1,2} ¹ W. M. Keck Research Laboratory in Astrochemistry, University of Hawaii at Manoa, Honolulu, HI 96822, USA² Department of Chemistry, University of Hawaii at Manoa, Honolulu, HI 96822, USA

Received 2019 October 4; revised 2019 December 7; accepted 2019 December 10; published 2020 January 20

Abstract

The processing of the simple hydrocarbon ice, acetylene (C_2H_2/C_2D_2), via energetic electrons, thus simulating the processes in the track of galactic cosmic-ray particles penetrating solid matter, was carried out in an ultrahigh vacuum surface apparatus. The chemical evolution of the ices was monitored online and in situ utilizing Fourier transform infrared spectroscopy (FTIR) and ultraviolet–visible spectroscopy and, during temperature programmed desorption, via a quadrupole mass spectrometer with an electron impact ionization source (EI-QMS) and a reflectron time-of-flight mass spectrometer utilizing single-photon photoionization (SPI-ReTOF-MS) along with resonance-enhanced multiphoton photoionization (REMPI-ReTOF-MS). The confirmation of previous in situ studies of ethylene ice irradiation using FTIR was accomplished with the detection of five products: ethane (C_2H_6/C_2D_6), ethylene (C_2H_4/C_2D_4), diacetylene (C_4H_2/C_4D_2), vinylacetylene (C_4H_4/C_4D_4), and benzene (C_6H_6/C_6D_6). Alternatively to previous gas-phase analytical studies, the sensitive SPI-ReTOF-MS analysis detected 10 hydrocarbon groups of distinct degrees of saturation: C_nH_{2n+2} ($n = 4, 6–16$), C_nH_{2n} ($n = 2, 3, 6, 8–16$), C_nH_{2n-2} ($n = 3, 4, 6, 8, 10–15$), C_nH_{2n-4} ($n = 4–8, 10–14$), C_nH_{2n-6} ($n = 4–10, 12–16$), C_nH_{2n-8} ($n = 6–10, 12, 14–17$), C_nH_{2n-10} ($n = 6–12, 14–17$), C_nH_{2n-12} ($n = 8–14$), C_nH_{2n-14} ($n = 8–16$), and C_nH_{2n-16} ($n = 10–16$). From these detected groups the REMPI-ReTOF-MS method was able to assign the isomer-specific production of five aromatic hydrocarbons: benzene (C_6H_6), phenylacetylene (C_8H_6), styrene (C_8H_8), naphthalene ($C_{10}H_8$), and phenanthrene ($C_{14}H_{10}$).

Unified Astronomy Thesaurus concepts: [Saturnian satellites \(1427\)](#); [Spectroscopy \(1558\)](#); [Mass spectrometry \(2094\)](#); [Polycyclic aromatic hydrocarbons \(1280\)](#); [Astrochemistry \(75\)](#); [Interstellar dust \(836\)](#)

1. Introduction

Acetylene (C_2H_2), the simplest representative of an alkyne, has been detected in the gas phase of the circumstellar envelope of the carbon star IRC 10216, near carbon stars in the LMC, in the accretion disk of the young star GV Tau in the L1524 molecular cloud, as well as in the GL 2591, W3 IRS, and OMC-1 IRc2 molecular clouds, in the young stellar objects AFGL 2136/2591/4176, NGC 3576/7538, W33 A, and W3 IRS 5, and toward the star-forming region Cepheus A East (Ridgway et al. 1976; Lacy et al. 1989; Lahuis & Van Dishoeck 2000; van Loon et al. 2006; Gibb et al. 2007; Sonnentrucker et al. 2007; Bast et al. 2013). In our solar system, acetylene is present in the coma of comets such as D/2012 S1 (ISON), C/2001 A2 (LINEAR), 9P (Tempel 1), 153P (Ikeya-Zhang), Lee, C/1995 O1 (Hale–Bopp), C/1996 B2 (Hyakutake), and 1P/Halley (Giotto NMS) (Brooke et al. 1996; Despois 1997; Sekiguchi et al. 1997; Crovisier et al. 2004; Mumma et al. 2005; DiSanti et al. 2016) and in hydrocarbon-rich atmospheres of planets and their moons such as Jupiter (Ridgway 1974; Carlson et al. 2016; Keane 2017), Saturn (Moses et al. 2000), and Saturn’s largest moon Titan (Coustenis et al. 2007). Acetylene was also identified as a solid on Titan’s surface (Singh et al. 2016). Titan is a unique object in the solar system, as it is the only body, besides Earth, to have a dense nitrogen-based atmosphere and a solid surface. Due to its similarity to Earth, Titan has been the subject of multiple remote observations such as with the *ISO* space telescope and ALMA (Coustenis et al. 2003; Palmer et al. 2017), as well as via flyby missions including *Pioneer 11*,

Voyager 1 and 2, and *Cassini*, which included the Huygens lander (Zarnecki et al. 2005). Beneath Titan’s atmosphere, exotic features such as liquid hydrocarbon lakes—likely containing methane, ethane, propane, and acetylene—exist owing to its cold surface temperature of about 94 K, and dark dunes consisting of organics have been detected. (Stofan et al. 2007; Brown et al. 2008; Cordier et al. 2009, 2013). Similarly, the *New Horizons* mission detected acetylene, via ultraviolet spectroscopy, in Pluto’s atmosphere and observed an increase in abundance at lower altitudes (Gladstone et al. 2016). This information, along with models of Pluto’s atmosphere utilizing *New Horizons* data, determined that acetylene was the top precipitating species (Wong et al. 2017), suggesting that, similar to Titan, acetylene ice could be present on Pluto’s surface. Furthermore, the *New Horizons* mission revealed large abundances of methane ice present on Pluto’s surface; it has been shown through laboratory studies that acetylene represents the major product of processed methane ices (Kaiser et al. 1992; Kaiser & Roessler 1998; Bennett et al. 2006; Mejía et al. 2013; Boogert et al. 2015). Therefore, it is likely that solid acetylene exists on Pluto’s surface as well. Finally, Makemake—a Kuiper Belt object (KBO)—also displays evidence for solid acetylene on its surface (Brown et al. 2015).

Acetylene represents an important precursor for the formation of complex hydrocarbons such as benzene (C_6H_6), which have been shown to form via solid-phase, nonequilibrium reactions from galactic cosmic rays (GCRs) interacting with acetylene ice (Zhou et al. 2010). Due to the cold surface temperature of Titan (94 K), thermal reactions are negligible

and chemical reactions need to be initiated by high-energy radiation such as by GCRs. High-energy GCRs can penetrate the atmosphere of Titan to the surface and produce secondary electrons upon interaction with Titan's surface ices, resulting in chemical modification of the simpler hydrocarbon into more complex hydrocarbons such as vinylacetylene (C_4H_4), butene (C_4H_8), *n*-butane (C_4H_{10}), and benzene (C_6H_6) (Vuitton et al. 2008; Wilson & Atreya 2009; Kim et al. 2010; Zhou et al. 2010).

Although the atmospheric chemistry of Titan has been studied extensively both experimentally and in models (Balucani et al. 2000b; Stahl et al. 2002; Gu et al. 2009; Zhang et al. 2009c; Cunshun et al. 2010; Jones et al. 2010; Kaiser et al. 2010a; Kaiser & Mebel 2012; Lindén et al. 2016; Hörst 2017; Linden et al. 2018; Jiménez-Redondo et al. 2019), the cold surface chemistry occurring has remained a mystery even though Titan's dark dunes—most likely consisting of complex hydrocarbons—have been shown to cover about 10%–20% of the surface, making these dunes the largest surface reservoirs of organics (Hörst 2017). Recently, *Cassini*'s Visible and Infrared Mapping Spectrometer data revealed that solid acetylene is present, via its 1.55 and 4.93 μm absorption bands, at Titan's low-albedo equatorial regions Shangri La and Fensal-Aztlan/Quivira, but not in the higher-albedo equatorial area of Tui Regio (Singh et al. 2016). These low-albedo regions correspond to Titan's dunes—as seen by the *Cassini* Synthetic Aperture Radar Imager (SAR; 13.78 GHz/2.17 cm Ku-band) on 18 flybys—and the detection of acetylene in the same region as the dunes, *but not in the higher-albedo region*, strongly suggests that acetylene is directly related to the formation of Titan's dark dune material (Lorenz et al. 2006; Lunine & Hörst 2011). Nevertheless, despite the detection of solid acetylene—and the knowledge that acetylene acts as a precursor to complex hydrocarbons under Titan's radiation conditions—a comprehensive analysis of the products formed from the irradiation of pure acetylene ice is lacking. This lack of detailed chemical information for Titan, along with its possible applicability to Pluto and KBOs, has necessitated the following studies.

Pure acetylene ices processed with vacuum ultraviolet (VUV) photons identified the products as polyynes up to icosadecyne ($C_{20}H_2$) (Cuyllé et al. 2014). Similarly, acetylene and deuterated acetylene, isolated in neon ices, processed with VUV photons identified the products ethynyl radical (C_2H), vinyl radical (C_2H_3), tricarbon (C_3), tetracarbon (C_4), butadiynyl (C_4H), 1, 3-butadiyne (C_4H_2), hexacarbon (C_6), octacarbon (C_8), and octatetrayne (C_8H_2) (Wu & Cheng 2008). Matrix isolated acetylene in nitrogen ices, processed with VUV photons, revealed the products ethynyl radical (C_2H), cyano radical (CN), and isocyanogen (C_2N_2) isomers, while electron irradiation produced ethynyl radical (C_2H), carbene (CH_2), vinyl radical (C_2H_3), 1, 3-butadiyne (C_4H_2), cyanomethylidyne (C_2N), cyanomethylene (HC_2N), diazocarbene (CN_2), cyanogen isomer (CNNC), diisocyanocarbene (C_3N_2), azide radical (N_3), and tetranitrogen (N_4) (Wu et al. 2014). Pure acetylene, as well as deuterated acetylene, ices processed with 150 eV electrons produced species identified as singly ionized C_3D_3 , C_6D_6 , C_7D_7 , $C_{10}D_8$, C_4D_2 , C_4D_3 , C_4D_4 , C_8D_6 , and C_9D_7 ; however, the authors note that these ions are not isomer specific (Floyd et al. 1973). Studies of pure acetylene ices processed with hydrogen and deuterium atoms identified the primary product as ethane (C_2H_6), but no detection of ethylene

(C_2H_4) was reported (Hiraoka et al. 2000; Hiraoka & Sato 2001). Acetylene ices processed with 9.0 MeV He^{2+} nuclei and 7.3 MeV protons (H^+) identified general acetylenic and olefenic species, along with the polycyclic aromatic hydrocarbons (PAHs) chrysene ($C_{18}H_{12}$), perylene ($C_{20}H_{12}$), pentacene ($C_{22}H_{14}$), and coronene ($C_{24}H_{12}$) as the products, as well as a residue after warming the substrate to room temperature (Kaiser & Roessler 1997, 1998). Pure acetylene ices processed with 200 keV H^+ ions identified the products as acetylenic and olefenic type species as carbon chains containing 8–12 carbon atoms, as well as a residue after warming the sample (Compagnini et al. 2009; Puglisi et al. 2014). Pure acetylene ices processed with 30 keV He^+ and 15 keV N^+ ions produced features identified as mono-substituted acetylenic species and mono-nitriles including HCN, respectively, with the detection of a residue still present after heating the sample (Strazzulla et al. 2002). Processing acetylene (C_2H_2), as well as carbon-13 acetylene ($^{13}C_2H_2$) and deuterated acetylene (C_2D_2), ices with 5 keV electrons resulted in the detection of cumulenenic and vinylic species, along with the discrete molecules benzene (C_6H_6), vinylacetylene (C_4H_4), and methylenecyclopropane (C_4H_4) as well as a residue after warming the sample (Zhou et al. 2010). Noble gas (argon, krypton, or xenon) matrix isolated and neat acetylene ices processed with 20 keV X-rays identified dicarbon (C_2), ethynyl radicals (C_2H), tentatively butadiynyl (C_4H), diacetylene (C_4H_2), and vinylacetylene (C_4H_4) in the isolated experiments, while vinylacetylene, cumulenenic species, and tentatively substituted benzene species were detected in the processed pure acetylene ices (Ryazantsev et al. 2018).

These studies depended on techniques such as infrared spectroscopy, ultraviolet–visible (UV–VIS) spectroscopy, and quadrupole mass spectrometry utilizing an electron ionization source (EI-QMS). However, these methods alone are highly limited (Abplanalp et al. 2016a); infrared spectroscopy can only identify small molecules along with *functional groups* of complex molecule, but not discrete complex molecules; UV–VIS spectroscopy of solid samples often has broad spectra that overlap for complex hydrocarbons, and EI-QMS ionizes molecules and regularly causes substantial fragmentation of the molecular ion. Each of these techniques does not allow for specific isomers to be discriminated, and the complimentary more sophisticated analytical procedures utilizing photoionization coupled to a reflectron time-of-flight mass spectrometer (PI-ReTOF-MS) need to be employed. Here, the use of single-photon ionization coupled with a reflectron time-of-flight mass spectrometer (SPI-ReTOF-MS) provides an ideally fragment-free analysis of the products subliming from the processed ice (Kaiser et al. 2015; Tarczay et al. 2016, 2017). Furthermore, by tuning the energy of the photons used to photoionize the subliming molecules, specific isomers can be unambiguously identified (Abplanalp et al. 2015, 2016b, 2018a; Förstel et al. 2016d; Maksyutenko et al. 2016; Bergantini et al. 2018d; Frigge et al. 2018a; Zhu et al. 2018). However, for complex molecules, isomers can often have overlapping ionization energies, but with resonance-enhanced multiphoton photoionization reflectron time-of-flight mass spectrometry (REMPI-ReTOF-MS), isomer-specific identification is still possible via the aid of unique resonance lines (Abplanalp et al. 2019). When the PI-ReTOF-MS techniques are coupled with Fourier transform infrared (FTIR) spectroscopy, UV–VIS spectroscopy, and EI-QMS, a new wealth of information that has remained elusive to previous pure acetylene irradiation experiments can be extracted. These results provide insights

into the hydrocarbon chemistry available at the surface of Titan and reveal an alternative pathway from atmospheric sources for the production of complex hydrocarbons via GCR-generated secondary electrons upon interaction with Titan's surface ices (Vuitton et al. 2008; Wilson & Atreya 2009; Kim et al. 2010; Zhou et al. 2010).

2. Experimental

The experiments were carried out in a stainless steel ultrahigh vacuum (UHV) chamber operating at pressures of 3×10^{-11} torr (Bennett et al. 2013; Jones & Kaiser 2013; Kaiser et al. 2014). The substrate, a polished rhodium-coated silver mirror, is mounted in the UHV chamber to a cryostat via indium foil for thermal conductivity and is cooled to 5.0 ± 0.1 K. The closed cycle helium cryostat (Sumitomo, RDK-415E) is able to be rotated in the horizontal plane or repositioned in the vertical plane of the UHV chamber utilizing its differentially pumped rotary feedthrough (Thermionics Vacuum Products, RNN-600/FA/MCO) and UHV compatible bellow (McAllister, BLT106), respectively. Once the substrate has been cooled, acetylene (C_2H_2 , AirGas, >99.9%) was deposited onto the substrate via a glass capillary array, positioned 30 mm away, using a background pressure of 5×10^{-8} torr over a few minutes (Maity et al. 2014a, 2014b, 2015). Trace amounts of the acetone (CH_3COCH_3) stabilizer were eliminated quantitatively from the acetylene via a dry ice-ethanol slush bath. The acetylene deposition was monitored online and in situ via laser interferometry by reflecting an HeNe laser ($\lambda = 632.8$ nm; CVI Melles-Griot; 25-LHP-230) off of the silver mirror into a photodiode (Groner et al. 1973; Turner et al. 2015, 2016). Utilizing acetylene's refractive index (n) of 1.34 (Hudson et al. 2014) and the recorded interference fringes allows for a precise determination of the ice thickness, which was calculated to be 750 ± 60 nm. The ice thickness was also determined via a modified Lambert-Beer relationship utilizing the integrated areas for the acetylene's infrared vibrations at 6465 ($\nu_1 + \nu_3$), 4072 ($\nu_1 + \nu_5$), 3862 ($\nu_2 + 2\nu_4 + \nu_5$), 3328 (ν_1), 3240 (ν_3), 1371 ($\nu_4 + \nu_5$), and 742 ($\nu_6 + \nu_{10}$). Using acetylene's absorption coefficients of 4.20×10^{-19} , 2.30×10^{-19} , 2.10×10^{-19} , 5.90×10^{-19} , 2.39×10^{-17} , 3.10×10^{-18} , and 2.42×10^{-17} cm molecule $^{-1}$ resulted in an average thickness of 600 ± 100 nm, which lies within the range of the more accurate laser interferometry method (Hudson et al. 2014; Table 1). Deuterium isotopically substituted D2-acetylene (C_2D_2 , C.D.N. Isotopes, 99% D) ices, with similar thicknesses of 780 ± 60 nm, were also used to confirm both infrared spectroscopy and mass spectrometry assignments via the observed isotopic shifts (Table 2; Frigge et al. 2018b; Turner et al. 2018).

Following deposition of the desired ice thickness, the acetylene ice was analyzed in situ before, during, and after processing with an FTIR spectrometer (Nicolet 6700) and a UV-VIS spectrometer (Nicolet Evolution 300). The FTIR spectrometer was operated in absorption-reflection-absorption mode at a reflection angle of 45° and monitored the infrared region of $5000\text{--}500$ cm $^{-1}$, using a resolution of 4 cm $^{-1}$, which results in 22 spectra to be accumulated during the irradiation of the ice with 5 keV electrons (Figure 1; Kaiser & Maksyutenko 2015b; Maksyutenko et al. 2015; Förstel et al. 2016a). Before and after the irradiation, the infrared region of $10,000\text{--}5000$ cm $^{-1}$ was also recorded (Figure 1). Simultaneously, the focused light of the

UV-VIS spectrometer was reflected off of the rhodium-coated silver mirror at an angle of 30° and focused onto a photodiode that is shielded from ambient light. Here, the absorption spectra in the range of $190\text{--}1100$ nm was recorded with a resolution of 4 nm and a scan speed of 120 nm minute $^{-1}$, recording eight spectra during the irradiation phase (Figure 2). Rhodium coating increases the reflectivity in this wavelength regime, as it eliminates the possibility of absorption due to pure silver at approximately 320 nm (Jones et al. 2014a). FTIR analysis allowed for the vibrational modes of the reactants and products to be monitored during the experiment, while UV-VIS probed the electronic transitions present.

The irradiation phase consisted of 5 keV electrons processing 1.0 ± 0.1 cm 2 of the acetylene ice, at an incidence angle of 70° relative to the surface normal of the mirror, for 45 minutes at a current of 30 nA, mimicking the secondary electrons produced when GCRs penetrate interstellar ices (Zheng et al. 2006; Kaiser et al. 2013; Jones et al. 2014a, 2014b). CASINO 2.42 software was used, along with the densities of acetylene (C_2H_2 , $\rho = 0.76 \pm 0.08$ g cm $^{-3}$) and D2-acetylene (C_2D_2 , $\rho = 0.89 \pm 0.09$ g cm $^{-3}$), to determine the penetration depth and dose deposited via the energetic electrons into the ice (van Nes 1978; McMullan et al. 1992; Drouin et al. 2007; Góbi et al. 2016, 2017a, 2017b, 2017c). Here, the electrons were calculated to deliver an average dose of 3.1 ± 0.6 and 3.4 ± 0.7 eV molecule $^{-1}$ and penetrate to an average depth of 370 ± 50 and 310 ± 40 nm into the acetylene (C_2H_2) and D2-acetylene (C_2D_2) ices, respectively, which are less than the experimentally measured ice thickness and ensure no interaction between the electrons and the substrate (Table 3).

Upon completion of irradiation, the ice is kept isothermal at 5 K for 1 hr, and then temperature programmed desorption (TPD) studies were carried out by heating the substrate to 300 K at a rate of 0.5 K minute $^{-1}$ (Bergantini et al. 2017; Förstel et al. 2017; Tsegaw et al. 2017). The FTIR and UV-VIS simultaneously and continuously monitor the ice during the TPD phase (Figures 3 and 4), and the subliming molecules are analyzed with a quadrupole mass spectrometer (QMS; Extrel, Model 5221) (Figure 5) and the PI-ReTOF-MS technique (Figure 6). The QMS utilizes an electron impact ionizer operating at 70 eV and an emission current of 1 mA to monitor the mass range from 1 to 200 amu during TPD. Meanwhile, the SPI-ReTOF-MS system also detects the subliming molecules by first using single-photon ionization via pulsed coherent VUV light at an energy of 10.49 eV ($\lambda = 118.2$ nm) and a typical flux of $(5.0 \pm 0.5) \times 10^{12}$ photons s $^{-1}$ to ionize the molecule, and then the ions are detected utilizing a modified reflectron time-of-flight mass spectrometer (Jordan TOF products, Inc.) (Kaiser & Maksyutenko 2015a; Förstel et al. 2016c; Bergantini et al. 2018b, 2018c). The photoionization energy of 10.49 eV is utilized owing to its capability of ionizing most hydrocarbons (Abplanalp & Kaiser 2016, 2017; Abplanalp et al. 2018c).

In detail for SPI-ReTOF-MS, the VUV light is generated by nonresonant four-wave mixing from frequency tripling the third harmonic output of an Nd:YAG laser (355 nm) via xenon gas (99.999% Praxair) used as a nonlinear medium (Bergantini et al. 2018a; Góbi et al. 2018). Here, a pulse valve introduces a xenon gas jet into which the 355 nm light is focused. The interaction of the intense laser pulses with the nonlinear xenon gas medium produces 118 nm (10.49 eV) light that is then

Table 1
Infrared Absorption Features Recorded before and after the Irradiation of Acetylene Ices (C_2H_2) at 5 K

Absorptions before Irradiation (cm^{-1})	Absorptions after Irradiation (cm^{-1})	Assignment	Carrier	References
6465, 5174		$\nu_1 + \nu_3, 5\nu_4 + 3\nu_5$ (C_2H_2)	Combination	1
4076, 3948, 3863		$\nu_1 + \nu_5, 2\nu_2, \nu_2 + 2\nu_4 + \nu_5$ (C_2H_2)	Combination/overtone	1
3328		ν_1 (C_2H_2)	CH stretch	1
	3320	ν_4 (C_4H_2)	CH stretch	2
	3280	ν_1 (C_4H_4)/ ν_{CH} ($R-C\equiv CH$)	CH stretch	3, 4, 5
3235		ν_3 (C_2H_2)	CH stretch	1
	3154	ν_{CH} ($R-CHCH_2$)	CH_2 asymmetric stretch	5, 6
	3094	ν_9 (C_2H_4)	CH_2 asymmetric stretch	7
	^a 3030	ν_{18} (C_6H_6)/ ν_{CH} (Aromatic)	Overtone/aromatic CH stretch	6, 8, 9, 10, 11
3005		ν_3 ($^{13}C_2H_2$)	CH stretch	1
	2974	ν_{10} (C_2H_6)/ ν_{11} (C_2H_4)/ $\nu_6 + \nu_7$ (C_4H_4)	CH_3 degenerate stretch/ CH_2 symmetric stretch/ combination	5, 7
	2884	ν_5 (C_2H_6)	CH_3 symmetric stretch	12
2735, 2708		$\nu_2 + \nu_5$ (C_2H_2)	Combination	13, 14
2545		ν_3 (C_2DH)	CD stretch	13
	2090	ν ($C\equiv C\equiv C$)	Asymmetric stretch	15
1961		ν_2 (C_2H_2)	$C\equiv C$ stretch	14
	1951	ν ($C=C=C$)	Asymmetric stretch in $RCH=C=CH_2$	5
	1600	ν_6 (C_4H_4)	$C=C$ stretch	3, 5, 16
1389		$\nu_4 + \nu_5$ (C_2H_2)	Combination	13
	1240	$2\nu_{17}$ (C_4H_4)/ $\nu_6 + \nu_8$ (C_4H_2)	Overtone/combination	2, 3, 5, 14
	^a 1010–890	ν_{20} (C_6H_6)/ ν_{CH} (aromatic)	Out-of-plane CH deformation modes in substituted benzenes and PAHs	4, 8, 9, 10, 17, 18, 19
741		ν_5 (C_2H_2)	CCH bend	1
	690	ν_{11} (C_6H_6)	CH bend	5

Note.

^a See Abplanalp et al. (2019).

References. (1) Hudson et al. 2014b; (2) Zhou et al. 2009a; (3) Cuyllé et al. 2014; (4) Kaiser & Roessler 1998; (5) Zhou et al. 2010; (6) Allamandola et al. 1989; (7) Abplanalp & Kaiser 2017; (8) Kaiser & Roessler 1997; (9) McMurtry et al. 2016; (10) Sandford et al. 2004; (11) Zhang & Sander 2017; (12) Abplanalp et al. 2018c; (13) Bottger & Eggers 1964; (14) Doney et al. 2018; (15) Duley & Anming 2009; (16) Kim & Kaiser 2009; (17) Cané et al. 1997; (18) Hudgins & Sandford 1998; (19) Kaiser et al. 1997; (20) Wu & Cheng 2008; (21) Törneng et al. 1980; (22) Bauschlicher et al. 1997; (23) Cané et al. 2007; (24) Hudgins et al. 1994; (25) Hollenberg & Dows 1962; (26) Abplanalp & Kaiser 2016.

separated from the 355 nm light via a lithium fluoride (LiF) lens based on their difference in refractive index (Förstel et al. 2015, 2016b). The LiF lens also focuses the selected wavelength and directs it to a position of about 1 cm above the ice to ionize subliming molecules. Once ionized, the ReTOF utilizes a multichannel plate in the dual-chevron configuration to detect the arriving ions. This signal was then amplified (Ortec 9305) and shaped using a 100 MHz discriminator. The resulting spectra are then recorded with 4 ns bin widths and 3600 sweeps using a multichannel scaler (FAST ComTec, P7888-1 E) triggered at 30 Hz (Quantum Composers, 9518), resulting in a single mass spectrum per 1 K change in temperature of the substrate (Figure 6).

Alternatively, one- and two-color REMPI was also utilized to isomer-selectively detect several of the subliming molecules. Here, REMPI first excites the molecule of interest into an intermediate state via a resonant photon absorption—unique to the isomer to be identified—which is then ionized by a second photon (Swenson & Gillispie 1996). First, ultraviolet (UV) light (258.994–341.054 nm) was produced by pumping a dye laser with an Nd:YAG laser to produce visible light (517.988–682.108 nm); this light was then frequency doubled or tripled utilizing BBO crystals to produce UV photons of a precise wavelength (± 0.001 nm). The REMPI-ReTOF-MS setup was confirmed to operate correctly utilizing carbon

monoxide (CO) to calibrate the system (Abplanalp et al. 2019). REMPI-ReTOF-MS was used for the isomer-specific detection of benzene (C_6H_6), phenylacetylene (C_8H_6), styrene (C_8H_8), naphthalene ($C_{10}H_8$), and phenanthrene ($C_{14}H_{10}$) via a one-color two-photon process [1 + 1]. For each molecule the REMPI study was carried out twice in order to first determine the wavelength at which maximum ionization occurred, and then repeated at the maximum REMPI wavelength determined from the wavelength scan. Similarly, a two-color two-photon [1+1'] REMPI scheme was used to confirm the presence of phenanthrene, which operates as described above, except that the first (341.054 nm) and second (287.202 nm) photons have different wavelengths and therefore different energies.

3. Results

3.1. FTIR and UV–VIS Spectroscopy

FTIR analysis detected multiple individual irradiation products, as well as intensity increases and broadening of vibrations assigned to acetylene; the latter most likely indicates the formation of products with overlapping vibration modes. Figure 1 displays the FTIR spectrum before and after processing in the acetylene (C_2H_2) and D2-acetylene (C_2D_2) experiments, where new infrared stretches corresponding to new hydrocarbons

Table 2
Infrared Absorption Features before and after the Irradiation of D₂-acetylene Ices (C₂D₂) at 5 K

Absorptions before Irradiation (cm ⁻¹)	Absorptions after Irradiation (cm ⁻¹)	Assignment	Carrier	References
5015		$\nu_1 + \nu_3$ (C ₂ D ₂)	Combinations	13
3278		$\nu_1 + \nu_5$ (C ₂ D ₂)	Combinations	13
3244		ν_3 (C ₂ H ₂)	CH stretch	1
2925		$\nu_3 + \nu_4$ (C ₂ D ₂)	Combination	13
2680		ν_1 (C ₂ D ₂)	CD stretch	13
	2585	ν_4 (C ₄ D ₂)	CD stretch	20
	2573	ν_4 (C ₄ D ₄)	CD stretch	21
2544		ν_3 (C ₂ DH)	CD stretch	13
2400		ν_3 (C ₂ D ₂)	CD stretch	13
2341		ν_3 (¹³ C ₂ D ₂)	CD stretch	13
	2335	ν_9 (C ₂ D ₄)	CD ₂ asymmetric stretch	7
2320		$\nu_2 + \nu_5$ (C ₂ D ₂)	Combination	13
	^a 2265	ν_{18} (C ₆ D ₆)/ ν_{CD} (Aromatic)	CH stretch/aromatic CH stretch	22, 23, 24 25
	2230	ν_{10} (C ₂ D ₆)	CD ₃ degenerate stretch	26
	2192	ν_{11} (C ₂ D ₄)	CD ₂ symmetric stretch	7
1101		$2\nu_5$ (C ₂ D ₂)	Overtone	13
1085		$\nu_4 + \nu_5$ (C ₂ D ₂)	Combination	13
	^a 800–750	ν_{CD} (Aromatic)	Out-of-plane CH deformation modes in substituted benzenes and PAHs	17, 22, 23, 24
717		ν_5 (C ₂ H ₂)	CH bend	13
579		ν_5 (C ₂ D ₂)	CD bend	13

Note.

^a See Abplanalp et al. (2019).

References. (1) Hudson et al. 2014b; (2) Zhou et al. 2009a; (3) Cuylle et al. 2014; (4) Kaiser & Roessler 1998; (5) Zhou et al. 2010; (6) Allamandola et al. 1989; (7) Abplanalp & Kaiser 2017; (8) Kaiser & Roessler 1997; (9) McMurtry et al. 2016; (10) Sandford et al. 2004; (11) Zhang & Sander 2017; (12) Abplanalp et al. 2018c; (13) Bottger & Eggers 1964; (14) Doney et al. 2018; (15) Duley & Anming 2009; (16) Kim & Kaiser 2009; (17) Cané et al. 1997; (18) Hudgins & Sandford 1998; (19) Kaiser et al. 1997; (20) Wu & Cheng 2008; (21) Törneng et al. 1980; (22) Bauschlicher et al. 1997; (23) Cané et al. 2007; (24) Hudgins et al. 1994; (25) Hollenberg & Dows 1962; (26) Abplanalp & Kaiser 2016.

are readily visible. The discrete products identified with FTIR include ethane (C₂H₆, ν_5 2884 cm⁻¹/C₂D₆, ν_{10} 2230 cm⁻¹), ethylene (C₂H₄, ν_9 3094 cm⁻¹/C₂D₄, ν_9 2335 cm⁻¹), diacetylene (C₄H₂, ν_4 3320 cm⁻¹/C₄D₂, ν_4 2585 cm⁻¹), vinylacetylene (C₄H₄, ν_1 3280 cm⁻¹/C₄D₄, ν_4 2573 cm⁻¹), and benzene (C₆H₆, ν_{11} 690 cm⁻¹/C₆D₆, ν_{18} 2265 cm⁻¹) (Tables 1 and 2). However, vibrations corresponding to acetylenic and olefinic CH symmetric stretching (3280 cm⁻¹), as well as C=C=C asymmetric stretching (1951 cm⁻¹), were also detected. Finally, vibrations corresponding to aromatic hydrocarbons were also visible at 3030 cm⁻¹ and from 890 to 1010 cm⁻¹ that correspond to aromatic CH stretching and C–H out-of-plane bending, respectively. Utilizing FTIR alone, only tentative assignment and hence functional groups of these larger hydrocarbons can be proposed, because their fundamental vibrations overlap with multiple modes of unsaturated hydrocarbons.

Simultaneous to the FTIR analysis, the UV–VIS analyzed the acetylene ice prior to, during, and after irradiation. Here, new features were detected via an increase in the absorbance signal over the entire 190–1100 nm region, but distinct features were observed from 190 to 400 nm (Figure 2). These features can be tentatively assigned to polyynes (C₄H₂, 200–240 nm/C₆H₂, 245–295 nm/C₈H₂, 190–225 nm/C₁₀H₂, 218–250 nm/C₁₂H₂, 270–280 nm/C₁₄H₂, 290–300 nm/C₁₈H₂, 325–335 nm/C₂₀H₂, 345–350 nm) and aromatic molecules (benzene, C₆H₆, 180–210 nm/naphthalene, C₁₀H₈, 200–220 nm/phenanthrene, C₁₄H₁₀, 230–250 nm/pyrene, C₁₆H₁₀, 260–270 nm); both polyynes and aromatic hydrocarbons have strong electronic transitions in this region

($\pi \rightarrow \pi^*$) (Cataldo 2004; Halasinski et al. 2005; Jolly & Benilan 2008; Cuylle et al. 2014; Dawes et al. 2017). The assignments of diacetylene (C₄H₂), vinylacetylene (C₄H₄), and benzene (C₆H₆) are all supported by their FTIR detection and have been suggested by previous studies (Zhou et al. 2010; Cuylle et al. 2014).

FTIR analysis of the processed acetylene ice during the TPD phase shows further evidence that higher molecular weight hydrocarbons were formed owing to infrared absorptions still being detected above 100 K (Figure 3). It is important to point out that none of the infrared absorptions observed increased in intensity during TPD, showing that these molecules were solely produced at 5 K and did not form during heating. Figure 3 displays the infrared spectra of the acetylenic C–H vibration during TPD from 100 to 300 K in increments of 20 K and shows that many complex hydrocarbons were produced as the infrared peak persists beyond 200 K. At 100 K the acetylene ice has already sublimed, and any remaining infrared absorptions are due to product molecules. However, even the larger hydrocarbons assigned with acetylenic vibrations (C₄H₂, C₄H₄) have sublimation temperatures below 200 K, but the peak at 3280 cm⁻¹ is still observable above 200 K. Relatedly, the UV–VIS analysis during TPD corroborated that larger hydrocarbons were present, as absorptions were still detectable above 100 K (Figure 4). During heating from 100 to 140 K, the UV–VIS absorptions from 190 to 250 nm decreased (Figures 4(a)–(c)). Meanwhile, the UV–VIS absorptions from 250 to 400 nm remained constant until 150 K, at which point they also began

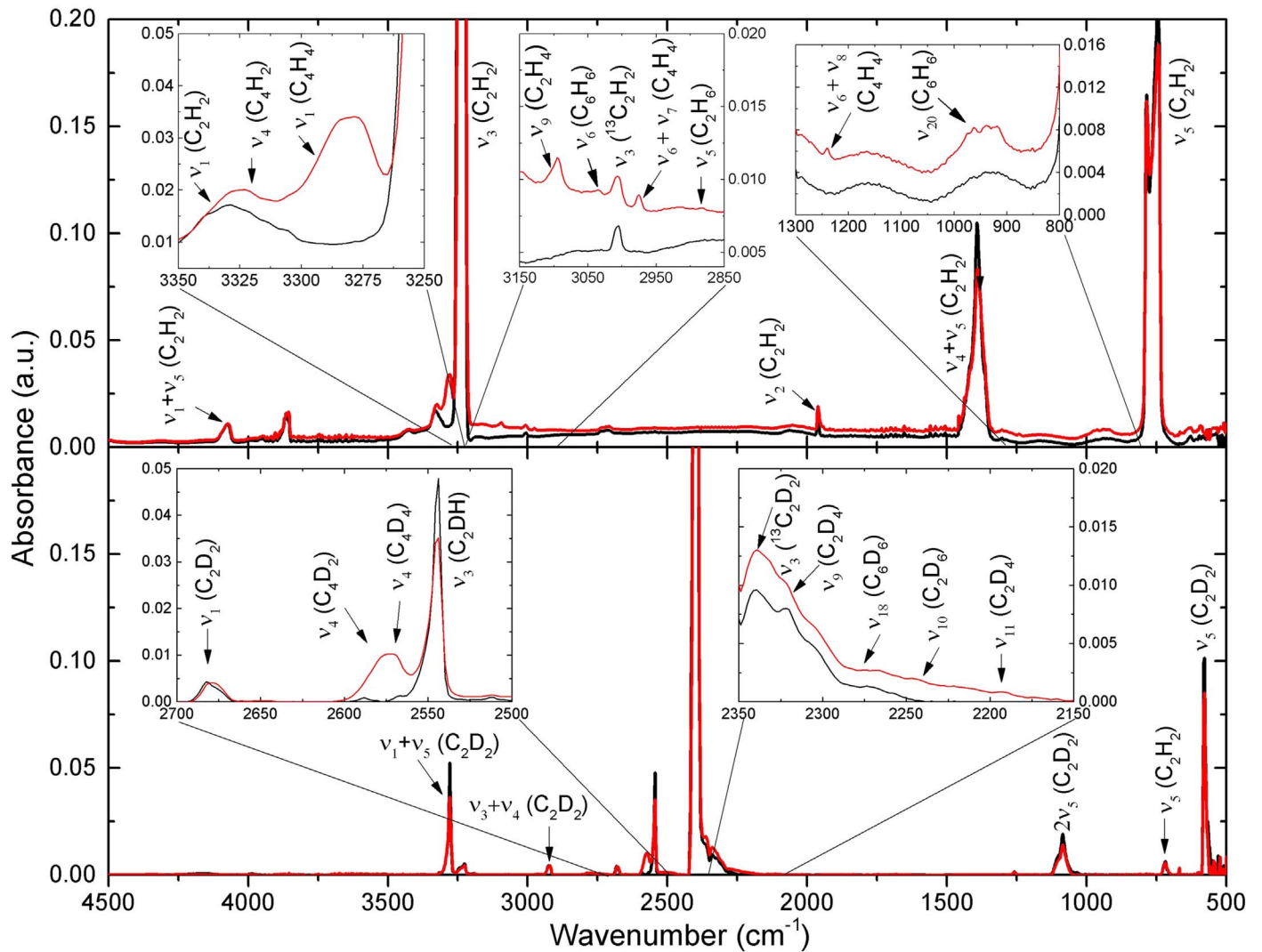


Figure 1. Infrared spectra from 4500 to 500 cm^{-1} for acetylene (C_2H_2 ; top) and D2-acetylene (C_2D_2 ; bottom) ices before (black) and after (red) the electron irradiation with assignments (Tables 1 and 2).

to decrease and lost intensity until 300 K was reached (Figures 4(d)–(f)). Finally, after heating the substrate to 300 K, a residue was detected by both FTIR and UV–VIS spectroscopy. To determine the identity of these larger molecules, the use of the complimentary analysis method of PI-ReTOF-MS during TPD provides further information on these hydrocarbons, as the changes in the FTIR and UV–VIS can be correlated with the detected ions.

3.2. Mass Spectrometry–PI-ReTOF-MS

The subliming molecules from the irradiated acetylene and D2-acetylene detected via SPI-ReTOF-MS at 10.49 eV are summarized in Figures 6–11. Figure 6 displays the signal intensity of detected ions versus temperature during TPD of the processed acetylene and D2-acetylene ices with mass-to-charge ratios greater than 250. Here, 10 groups of hydrocarbons with the following general formulae can be identified: $\text{C}_n\text{H}_{2n+2}$ ($n = 4, 6–16$), C_nH_{2n} ($n = 2, 3, 6, 8–16$), $\text{C}_n\text{H}_{2n-2}$ ($n = 3, 4, 6, 8, 10–15$), $\text{C}_n\text{H}_{2n-4}$ ($n = 4–8, 10–14$), $\text{C}_n\text{H}_{2n-6}$ ($n = 4–10, 12–16$), $\text{C}_n\text{H}_{2n-8}$ ($n = 6–10, 12, 14–17$), $\text{C}_n\text{H}_{2n-10}$ ($n = 6–12, 14–17$), $\text{C}_n\text{H}_{2n-12}$ ($n = 8–14$), $\text{C}_n\text{H}_{2n-14}$ ($n = 8–16$), $\text{C}_n\text{H}_{2n-16}$

($n = 10–16$). These generic groups were found to contain ion signals that correspond to molecules never before detected in acetylene irradiation experiments, and these data reveal several interesting trends previously unobserved. Ion signals can only be assigned to a specific molecular formula if a signal is detected for both isotopologues. Several of these ion signals also correspond to astrophysically important aromatic-ring-containing molecules such as at $m/z = 78$ (C_6H_6^+), 102 (C_8H_6^+), 104 (C_8H_8^+), 128 ($\text{C}_{10}\text{H}_8^+$), and 178 ($\text{C}_{14}\text{H}_{10}^+$), which could correspond to benzene (IE = 9.244 ± 0.001 eV), phenylacetylene (IE = 8.825 ± 0.001 eV), styrene (IE = 8.464 ± 0.001 eV), naphthalene (IE = 8.144 ± 0.001 eV), and phenanthrene (IE = 7.891 ± 0.001 eV) or anthracene (IE = 7.439 ± 0.006 eV). However, these isomers' ionization energies are overlapping with several of their isomers' ionization energies, and REMPI-ReTOF-MS was needed to unravel the true identity of these ion signals.

3.2.1. $\text{C}_n\text{H}_{2n+2}$

The mass-to-charge ratios corresponding to alkanes ($\text{C}_n\text{H}_{2n+2}$) of $n = 4, 6–16$ were detected using SPI-ReTOF-MS (Figure 7, left). The smaller alkanes methane (CH_4), ethane (C_2H_6), and

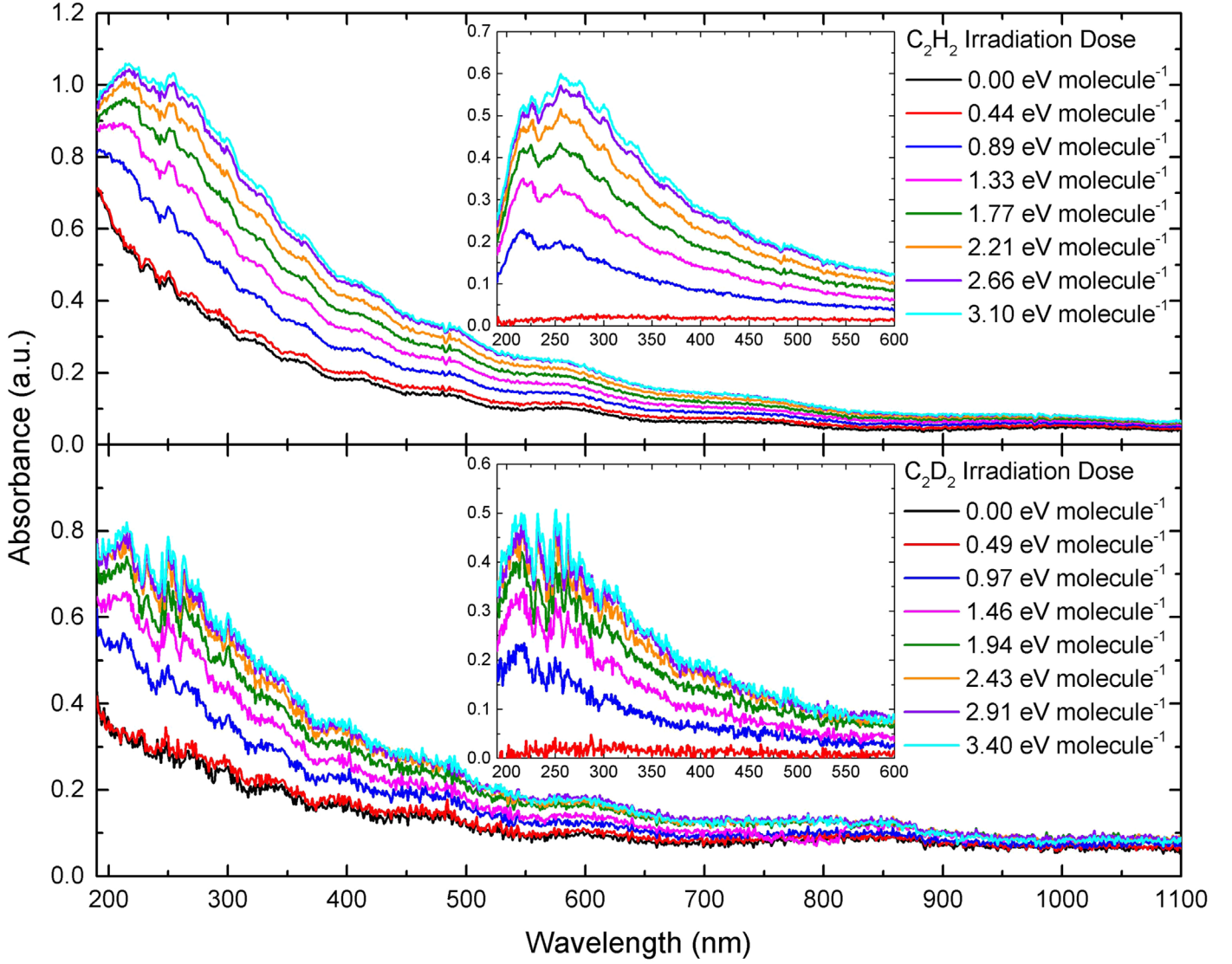


Figure 2. UV-VIS spectra from 190 to 1100 nm collected during irradiation for acetylene (C_2H_2 ; top) and D2-acetylene (C_2D_2 ; bottom). The insets show the difference spectra for each system with the unirradiated acetylene absorption subtracted.

Table 3
Data Applied to Calculate the Irradiation Dose per Molecule in the C_2H_2 and C_2D_2 Ice

Parameter	C_2H_2	C_2D_2
Irradiation current, I (nA)	30 ± 2	30 ± 2
Initial kinetic energy of the electrons, E_{init}	5 keV	5 keV
Total number of electrons	$(5.1 \pm 0.5) \times 10^{14}$	$(5.1 \pm 0.5) \times 10^{14}$
Average penetration depth, l^a (nm)	370 ± 50	310 ± 40
Density of the ice, ρ ($g\ cm^{-3}$)	0.76 ± 0.08	0.89 ± 0.09
Average kinetic energy of transmitted electrons, E_{trans}^a (keV)	0.8 ± 0.1	0.5 ± 0.1
Average kinetic energy of backscattered electrons, E_{bs}^a (keV)	3.2 ± 0.4	3.2 ± 0.4
Fraction of transmitted electrons, f_{trans}^a	0.00 ± 0.01	0.00 ± 0.01
Fraction of backscattered electrons, f_{bs}^a	0.32 ± 0.03	0.32 ± 0.03
Irradiated area, A (cm^2)	1.0 ± 0.1	1.0 ± 0.1
Dose per acetylene molecule (eV)	3.1 ± 0.6	3.4 ± 0.7
Total # molecules processed	$(6.4 \pm 1.6) \times 10^{17}$	$(6.0 \pm 1.5) \times 10^{17}$

Note.

^a CASINO output values.

propane (C_3H_8) products could not be detected via SPI-ReTOF-MS since their ionization energies of 12.61, 11.52, and 10.94 eV (Lias et al.), respectively, are higher than the 10.49 eV used

in the present experiments. However, larger alkanes were detected at $m/z = 58$ ($C_4H_{10}^+$, 131 K), $m/z = 86$ ($C_6H_{14}^+$, 145 K), $m/z = 100$ ($C_7H_{16}^+$, 153 K), $m/z = 114$ ($C_8H_{18}^+$,

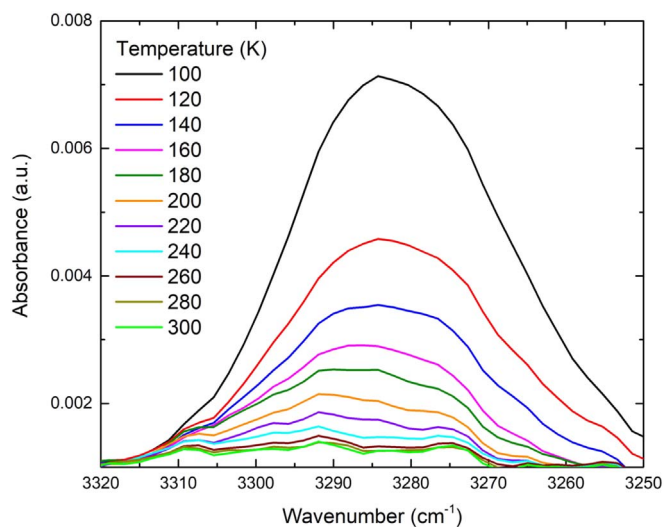


Figure 3. Infrared spectra of the new acetylenic C–H vibration ($3320\text{--}3250\text{ cm}^{-1}$) for irradiated acetylene (C_2H_2) during heating, after the reactant acetylene has sublimed.

168 K), $m/z = 128$ ($\text{C}_9\text{H}_{20}^+$, 166 K), $m/z = 142$ ($\text{C}_{10}\text{H}_{22}^+$, 175 K), $m/z = 156$ ($\text{C}_{11}\text{H}_{24}^+$, 182 K), and tentatively $m/z = 170$ ($\text{C}_{12}\text{H}_{26}^+$, 196 K), $m/z = 184$ ($\text{C}_{13}\text{H}_{28}^+$, 216 K), $m/z = 198$ ($\text{C}_{14}\text{H}_{30}^+$, 236 K), $m/z = 212$ ($\text{C}_{15}\text{H}_{32}^+$, 240 K), and $m/z = 226$ ($\text{C}_{16}\text{H}_{34}^+$, 243 K). Although these ion signals are possibly due to alkanes, their sublimation temperatures and profiles match other unsaturated hydrocarbon species much better in several cases, and only $m/z = 58$ can be definitively assigned to n-butane with the 10.49 eV data (see following sections). Overall these ion signals display the generally expected trend of increasing sublimation temperature with increasing molecular weight.

3.2.2. C_nH_{2n}

Observed alkenes (C_nH_{2n}) or the double-bond equivalent (D.B.E.) (cycloalkanes) of $n = 2, 3, 6, 8\text{--}16$ were probed as well (Figure 7, right). Similarly to the alkanes observed, several unsaturated hydrocarbons were detected at $m/z = 28$ (C_2H_4^+ , 80 K), $m/z = 42$ (C_3H_6^+ , 86 K), $m/z = 84$ ($\text{C}_6\text{H}_{12}^+$, 142 K), $m/z = 112$ ($\text{C}_8\text{H}_{16}^+$, 171 K), $m/z = 126$ ($\text{C}_9\text{H}_{18}^+$, 175 K), $m/z = 140$ ($\text{C}_{10}\text{H}_{20}^+$, 179 K), $m/z = 154$ ($\text{C}_{11}\text{H}_{22}^+$, 184 K), $m/z = 168$ ($\text{C}_{12}\text{H}_{24}^+$, 197 K), $m/z = 182$ ($\text{C}_{13}\text{H}_{26}^+$, 204 K), and tentatively $m/z = 196$ ($\text{C}_{14}\text{H}_{28}^+$, 220 K), $m/z = 210$ ($\text{C}_{15}\text{H}_{30}^+$, 227 K), and $m/z = 224$ ($\text{C}_{16}\text{H}_{32}^+$, 250 K), i.e., an increase of the sublimation temperature of typically 4–23 K per CH_2 unit. Like the alkane ion signals, there are most likely multiple contributors to these signals, as other unsaturated formulae share similar profiles for several of the alkane ion signals detected here.

3.2.3. $\text{C}_n\text{H}_{2n-2}$

Although the FTIR analysis did not detect the presence of any alkynes larger than acetylene, several mass-to-charge ratios corresponding to alkynes ($\text{C}_n\text{H}_{2n-2}$) or the double-bond equivalent (D.B.E.) (dienes, cycloalkenes, bicycloalkanes) of $n = 3, 4, 6, 8, 10\text{--}15$ were identified (Figure 8, left). These ions were observed at $m/z = 40$ (C_3H_4^+ , 85 K), $m/z = 54$ (C_4H_6^+ , 92 K), $m/z = 82$ ($\text{C}_6\text{H}_{10}^+$, 133 K), $m/z = 110$ ($\text{C}_8\text{H}_{14}^+$, 167 K), $m/z = 138$ ($\text{C}_{10}\text{H}_{18}^+$, 175 K), $m/z = 152$ ($\text{C}_{11}\text{H}_{20}^+$,

182 K), $m/z = 166$ ($\text{C}_{12}\text{H}_{22}^+$, 197 K), $m/z = 180$ ($\text{C}_{13}\text{H}_{24}^+$, 205 K), $m/z = 194$ ($\text{C}_{14}\text{H}_{26}^+$, 223 K), and $m/z = 208$ ($\text{C}_{15}\text{H}_{28}^+$, 227 K). With each additional CH_2 unit, an increase in sublimation temperature by 4–18 K was observed. The lack of ion signals corresponding to odd-carbon-atom-containing molecules ($n = 5, 7, 9$) may provide some information about the formation pathways of these unsaturated products.

3.2.4. $\text{C}_n\text{H}_{2n-4}$

The next most highly unsaturated group detected in these experiments, based on SPI-ReTOF-MS and also detected via vinylacetylene (C_4H_4) in FTIR, had the general formula $\text{C}_n\text{H}_{2n-4}$ ($n = 4\text{--}8, 10\text{--}14$) (Figure 8, right) and can correspond to multiple different structures (yne-ene, trienes, cycloalkenes, bicycloalkenes). The ion signals related to this group were detected at $m/z = 52$ (C_4H_4^+ , 89 K), $m/z = 66$ (C_5H_6^+ , 115 K), $m/z = 80$ (C_6H_8^+ , 120 K), $m/z = 94$ ($\text{C}_7\text{H}_{10}^+$, 151 K), $m/z = 108$ ($\text{C}_8\text{H}_{12}^+$, 160 K), $m/z = 136$ ($\text{C}_{10}\text{H}_{16}^+$, 175 K), $m/z = 150$ ($\text{C}_{11}\text{H}_{18}^+$, 209 K), $m/z = 164$ ($\text{C}_{12}\text{H}_{20}^+$, 213 K), $m/z = 178$ ($\text{C}_{13}\text{H}_{22}^+$, 204 K), and $m/z = 192$ ($\text{C}_{14}\text{H}_{24}^+$, 216 K). The majority of these ion signals match well with their isotopically shifted counterparts, except for $m/z = 122, 136,$ and 150, suggesting that they have other primary contributors.

3.2.5. $\text{C}_n\text{H}_{2n-6}$

The SPI-ReTOF-MS also detected the hydrocarbon group $\text{C}_n\text{H}_{2n-6}$ ($n = 4\text{--}10, 12\text{--}16$) (Figure 9, left), and this group was also detected through FTIR analysis via diacetylene (C_4H_2). Ion signals at $m/z = 50$ (C_4H_2^+ , 93 K), $m/z = 64$ (C_5H_4^+ , 113 K), $m/z = 78$ (C_6H_6^+ , 115 K), $m/z = 92$ (C_7H_8^+ , 140 K), $m/z = 106$ ($\text{C}_8\text{H}_{10}^+$, 146 K), $m/z = 120$ ($\text{C}_9\text{H}_{12}^+$, 172 K), $m/z = 134$ ($\text{C}_{10}\text{H}_{14}^+$, 174 K), $m/z = 162$ ($\text{C}_{12}\text{H}_{18}^+$, 205 K), $m/z = 176$ ($\text{C}_{13}\text{H}_{20}^+$, 208 K), $m/z = 190$ ($\text{C}_{14}\text{H}_{22}^+$, 215 K), $m/z = 204$ ($\text{C}_{15}\text{H}_{24}^+$, 220 K), and tentatively $m/z = 218$ ($\text{C}_{16}\text{H}_{26}^+$, 225 K) were identified. Each additional CH_2 unit resulted in an increase in sublimation temperature by 2–26 K. Similar to the previous group, these ion signals all match well to their isotopically shifted signals.

3.2.6. $\text{C}_n\text{H}_{2n-8}$

The next SPI-ReTOF-MS-detected hydrocarbon group was $\text{C}_n\text{H}_{2n-8}$ ($n = 6\text{--}10, 12, 14\text{--}17$) (Figure 9, right), detected via signals at $m/z = 76$ (C_6H_4^+ , 123 K), $m/z = 90$ (C_7H_6^+ , 130 K), $m/z = 104$ (C_8H_8^+ , 140 K), $m/z = 118$ ($\text{C}_9\text{H}_{10}^+$, 159 K), $m/z = 132$ ($\text{C}_{10}\text{H}_{12}^+$, 165 K), $m/z = 160$ ($\text{C}_{12}\text{H}_{16}^+$, 195 K), $m/z = 188$ ($\text{C}_{14}\text{H}_{20}^+$, 216 K), $m/z = 202$ ($\text{C}_{15}\text{H}_{22}^+$, 220 K), $m/z = 216$ ($\text{C}_{16}\text{H}_{24}^+$, 229 K), and tentatively $m/z = 230$ ($\text{C}_{17}\text{H}_{26}^+$, 243 K). Here, an additional CH_2 unit produced an increase in sublimation temperature by 4–19 K. Once again, the trend previously observed of similar sublimation profiles to the isotopically shifted signals suggests that the primary component of these signals is due mainly to this unsaturated group.

3.2.7. $\text{C}_n\text{H}_{2n-10}$

In addition, an even more highly unsaturated hydrocarbon group detected via SPI-ReTOF-MS belonged to the general formula $\text{C}_n\text{H}_{2n-10}$ ($n = 6\text{--}12, 14\text{--}17$) (Figure 10, left). The ions corresponding to this group were detected at $m/z = 74$ (C_6H_2^+ , 132 K), $m/z = 88$ (C_7H_4^+ , 145 K), $m/z = 102$ (C_8H_6^+ , 149 K), $m/z = 116$ (C_9H_8^+ , 159 K), $m/z = 130$ ($\text{C}_{10}\text{H}_{10}^+$, 162 K),

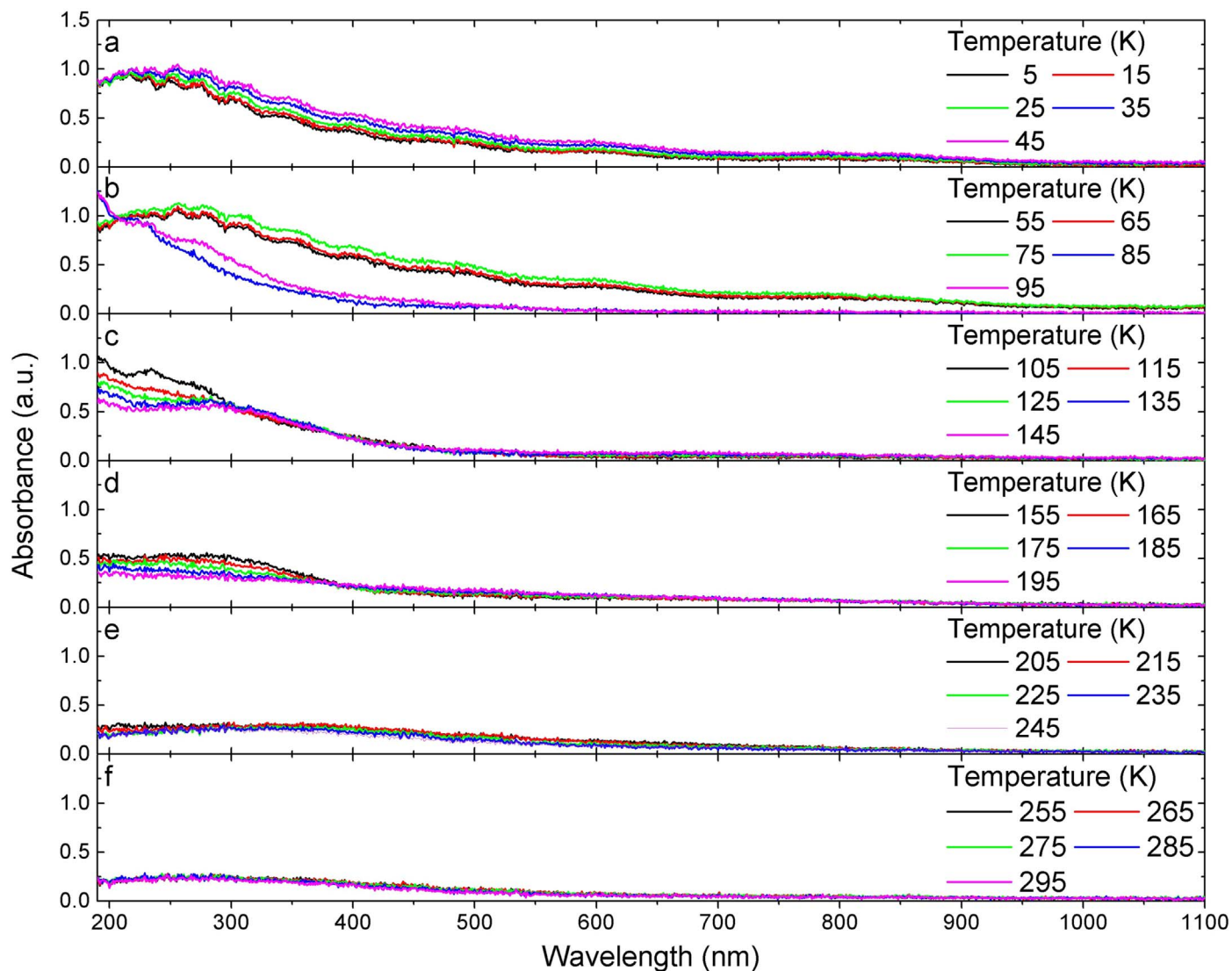


Figure 4. UV-VIS spectra from 190 to 1100 nm collected during heating, after irradiation of the acetylene ice (C_2H_2). Panel (a) ($T = 5\text{--}45$ K) displays the changes before acetylene sublimates. Panel (b) ($T = 55\text{--}95$ K) shows the acetylene phase change from amorphous to crystalline and the sublimation of acetylene. Panels (c) ($T = 105\text{--}145$ K), (d) ($T = 155\text{--}195$ K), and (e) ($T = 205\text{--}245$ K) show the slow decrease in absorbance of the remaining molecules. Panel (f) ($T = 255\text{--}295$ K) shows minimal changes in absorbance, but without a return to the baseline.

$m/z = 144$ ($C_{11}H_{12}^+$, 179 K), $m/z = 158$ ($C_{12}H_{14}^+$, 188 K), and tentatively $m/z = 186$ ($C_{14}H_{18}^+$, 216 K), $m/z = 200$ ($C_{15}H_{20}^+$, 221 K), $m/z = 214$ ($C_{16}H_{22}^+$, 225 K), and $m/z = 228$ ($C_{17}H_{24}^+$, 236 K). An additional CH_2 unit incorporated resulted in an increase in sublimation temperature by 3–17 K. Also, just as in the previous two groups, the deuterated ion signals have similar sublimation profiles. This continuing trend suggests that highly unsaturated hydrocarbons are the preferred product from acetylene irradiation.

3.2.8. C_nH_{2n-12}

The next hydrocarbon group detected belonged to the general formula C_nH_{2n-12} ($n = 8\text{--}14$) (Figure 10, right). The ions corresponding to this group were detected at $m/z = 100$ ($C_8H_4^+$, 161 K), $m/z = 114$ ($C_9H_6^+$, 166 K), $m/z = 128$ ($C_{10}H_8^+$, 168 K), $m/z = 142$ ($C_{11}H_{10}^+$, 175 K), $m/z = 156$ ($C_{12}H_{12}^+$, 182 K), and tentatively $m/z = 170$ ($C_{13}H_{14}^+$, 207 K) and $m/z = 184$ ($C_{14}H_{16}^+$, 210 K). An additional CH_2 unit incorporated resulted in an increase in sublimation temperature by 2–25 K. Interestingly, the

carbon chain length was detectable continuously from $n = 8\text{--}14$ for this group, suggesting that highly unsaturated hydrocarbons are a common product.

3.2.9. C_nH_{2n-14}

SPI-ReTOF-MS also detected ion signals corresponding to the general formula C_nH_{2n-14} ($n = 8\text{--}16$) (Figure 11, left). The ions corresponding to this group were detected at $m/z = 98$ ($C_8H_2^+$, 172 K), $m/z = 112$ ($C_9H_4^+$, 174 K), $m/z = 126$ ($C_{10}H_6^+$, 176 K), $m/z = 140$ ($C_{11}H_8^+$, 179 K), $m/z = 154$ ($C_{12}H_{10}^+$, 184 K), $m/z = 168$ ($C_{13}H_{12}^+$, 197 K), $m/z = 182$ ($C_{14}H_{14}^+$, 204 K), $m/z = 196$ ($C_{15}H_{16}^+$, 222 K), and tentatively $m/z = 210$ ($C_{16}H_{18}^+$, 225 K). The addition of each CH_2 unit resulted in an increase in sublimation temperatures by 2–18 K. Again, the carbon chain length was detectable continuously from $n = 8\text{--}16$ for this group, further suggesting that highly unsaturated hydrocarbons are a primary product of acetylene irradiation.

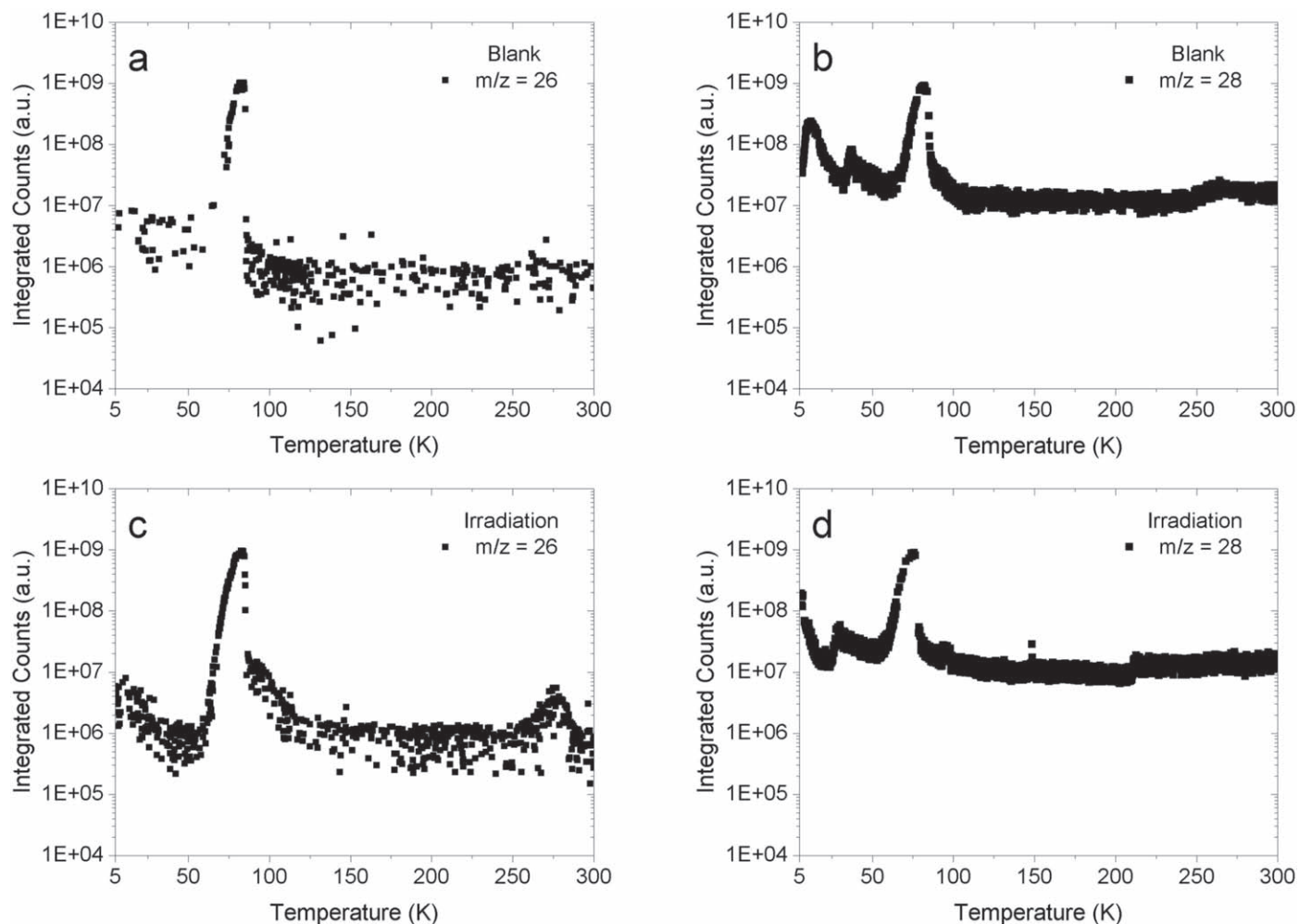


Figure 5. Sublimation profiles recorded during TPD via the EI-QMS for the (a, b) control experiment and (c, d) irradiation experiments of acetylene ($m/z = 26$; C_2H_2) and deuterated acetylene ($m/z = 28$; C_2D_2).

3.2.10. C_nH_{2n-16}

Finally, the most highly unsaturated hydrocarbon group detected belonged to the general formula C_nH_{2n-16} ($n = 10-16$) (Figure 11, right). The ion signals belonging to this group were revealed at $m/z = 124$ ($C_{10}H_4^+$, 174 K), $m/z = 138$ ($C_{11}H_6^+$, 177 K), $m/z = 152$ ($C_{12}H_8^+$, 180 K), $m/z = 166$ ($C_{13}H_{10}^+$, 195 K), $m/z = 180$ ($C_{14}H_{12}^+$, 205 K), $m/z = 194$ ($C_{15}H_{14}^+$, 220 K), and $m/z = 208$ ($C_{16}H_{16}^+$, 222 K). Each additional CH_2 unit incorporated resulted in an increase in sublimation temperature by 2–15 K. Similar to the previous hydrocarbon group, the carbon chain length was detectable continuously from $n = 10-16$.

3.2.11. REMPI-ReTOF-MS

The REMPI-ReTOF-MS wavelength scan for the ion signals $m/z = 78$ ($C_6H_6^+$), 102 ($C_8H_6^+$), 104 ($C_8H_8^+$), 128 ($C_{10}H_8^+$), and 178 ($C_{14}H_{10}^+$) was carried out utilizing maximum literature values of 258.986, 278.7, 287.4, 278.6, and 282.5/341.0 nm for benzene (C_6H_6), phenylacetylene (C_8H_6), styrene (C_8H_8), naphthalene ($C_{10}H_8$), and phenanthrene ($C_{14}H_{10}$), respectively, and revealed maximum values comparing very well to literature values (benzene = 258.994 nm, phenylacetylene = 278.801 nm,

styrene = 287.202 nm, naphthalene = 278.600 nm, and phenanthrene = 282.033/341.054 nm; Klimcak & Wessel 1980; Hager & Wallace 1988; Cockett et al. 1993; de la Cruz et al. 1994; Swenson & Gillispie 1996; Tzeng et al. 1999). Also, anthracene ($C_{14}H_{10}$) production was investigated via the $S_0 \rightarrow S_1$ transition (308–310 nm), but a scan from 300 to 312 nm revealed no signal. Nevertheless, anthracene may be produced at a yield below the detection limit, as its REMPI cross section is approximately two orders of magnitude less than phenanthrene’s $S_0 \rightarrow S_1$ REMPI transition (Adam et al. 2012). The sublimation profiles for $m/z = 78$ ($C_6H_6^+$), 102 ($C_8H_6^+$), 104 ($C_8H_8^+$), 128 ($C_{10}H_8^+$), and 178 ($C_{14}H_{10}^+$) produced at the maximum REMPI wavelength for each isomer were then able to be recorded, and they revealed signals that can only correspond to the aromatic hydrocarbons benzene (C_6H_6), phenylacetylene (C_8H_6), styrene (C_8H_8), naphthalene ($C_{10}H_8$), and phenanthrene ($C_{14}H_{10}$) (Figure 12). In Figure 12 the maximum intensity of the REMPI signal was scaled to lie on the same point relative to temperature as the SPI ion signal. This scaling allows for a clear depiction of what portion of the SPI ion signal belongs to the specific isomer ionized via REMPI and whether any other isomers contributed to the SPI signal.

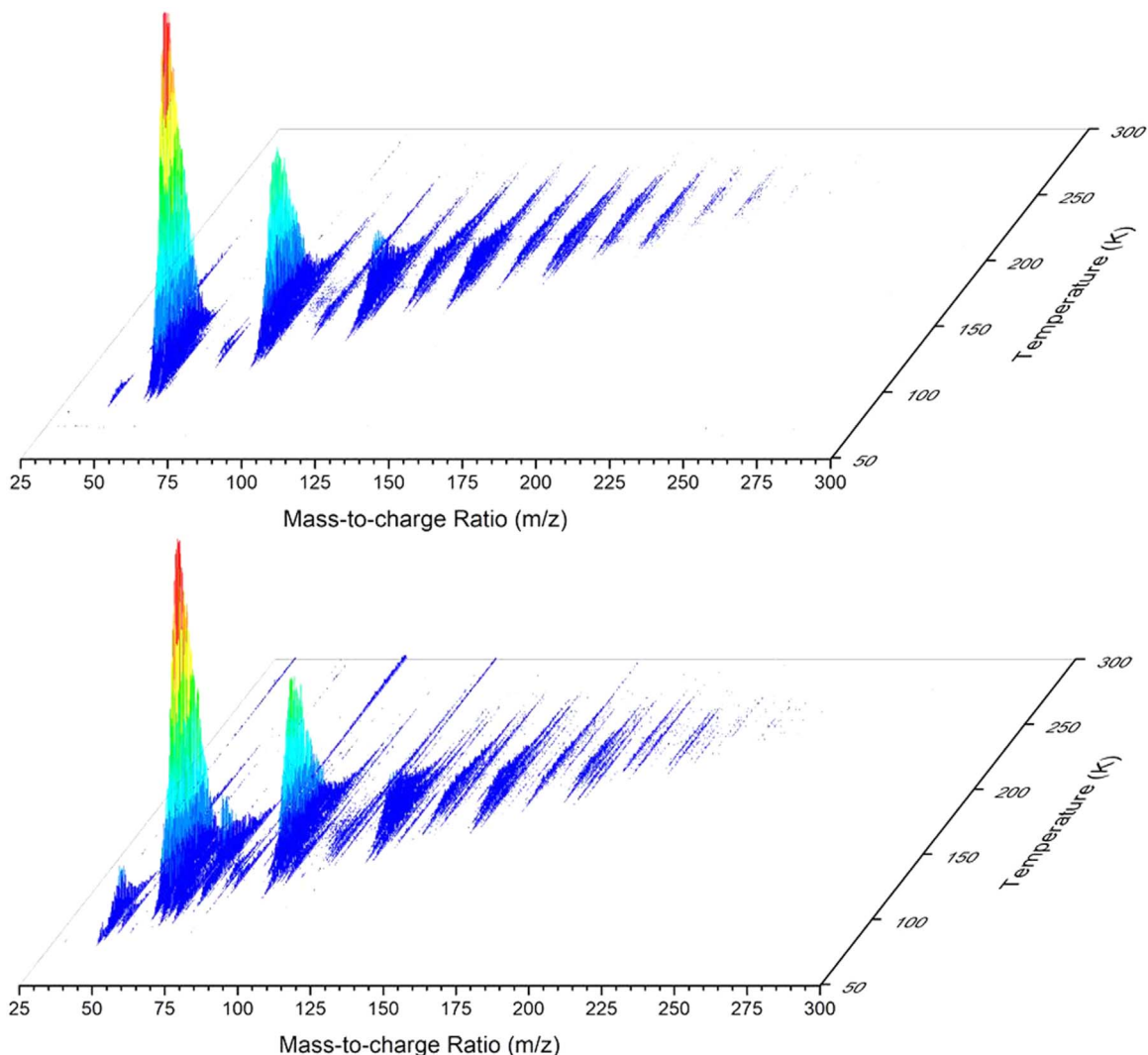


Figure 6. PI-ReTOF-MS data reporting the mass spectra vs. temperature at a photoionization energy of 10.49 eV for acetylene (C_2H_2 ; top) and D2-acetylene (C_2D_2 ; bottom).

3.3. Mass Spectrometry—QMS

Complimentary to the PI-ReTOF-MS techniques, the QMS operating in residual gas analyzer (RGA) mode was also able to monitor subliming molecules. However, as stated previously, this analytical method is less sensitive, and the facile fragmentation induced of these hydrocarbon products did not allow for any specific molecules to be identified. However, the RGA does provide insight into the acetylene (I.E. = 11.4 eV) sublimation profile, as its ionization energy is greater than 10.49 eV (Lias et al.). Figure 5 displays the difference in sublimation profiles during TPD of the acetylene ($C_2H_2^+$; $m/z = 26$; Figures 5(a), (c)) and deuterated acetylene ($C_2D_2^+$; $m/z = 28$; Figures 5(b), (d)) parent ions between the control or blank experiment and the irradiation experiment. Here, in both acetylene ices the irradiation experiment shows a broader sublimation peak, suggesting the formation of larger hydrocarbons that are inhibiting the sublimation of the acetylene, which agrees well with the PI-ReTOF-MS data.

4. Discussion

4.1. Summary of Results

Before continuing to the discussion of the results below, a brief summary of the results is compiled:

1. The FTIR analysis was able to detect five products: ethane (C_2H_6/C_2D_6), ethylene (C_2H_4/C_2D_4), diacetylene (C_4H_2/C_4D_2), vinylacetylene (C_4H_4/C_4D_4), and benzene (C_6H_6/C_6D_6) (Tables 1, 2; Figure 1).
2. The more sensitive SPI-ReTOF-MS study detected 10 hydrocarbon groups of distinct degrees of saturation: C_nH_{2n+2} ($n = 4, 6-16$), C_nH_{2n} ($n = 2, 3, 6, 8-16$), C_nH_{2n-2} ($n = 3, 4, 6, 8, 10-15$), C_nH_{2n-4} ($n = 4-8, 10-14$), C_nH_{2n-6} ($n = 4-10, 12-16$), C_nH_{2n-8} ($n = 6-10, 12, 14-17$), C_nH_{2n-10} ($n = 6-12, 14-17$), C_nH_{2n-12} ($n = 8-14$), C_nH_{2n-14} ($n = 8-16$), and C_nH_{2n-16} ($n = 10-16$).
3. The REMPI-ReTOF-MS results confirmed the isomeric production of five aromatic ringed hydrocarbons: benzene (C_6H_6), phenylacetylene (C_8H_6), styrene (C_8H_8), naphthalene ($C_{10}H_8$), and phenanthrene ($C_{14}H_{10}$).

4.2. C_nH_{2n+2}

The ion signals corresponding to the hydrocarbon group C_nH_{2n+2} with $n = 4, 6-16$ can belong to ions of alkanes (Figure 7). However, FTIR analysis was only able to determine the presence of ethane (C_2H_6) in the irradiated acetylene ice. Using the SPI-ReTOF-MS 10.49 eV data, the only alkane that can be isomer specifically identified is n-butane (I.E. = 10.5 ± 0.1),

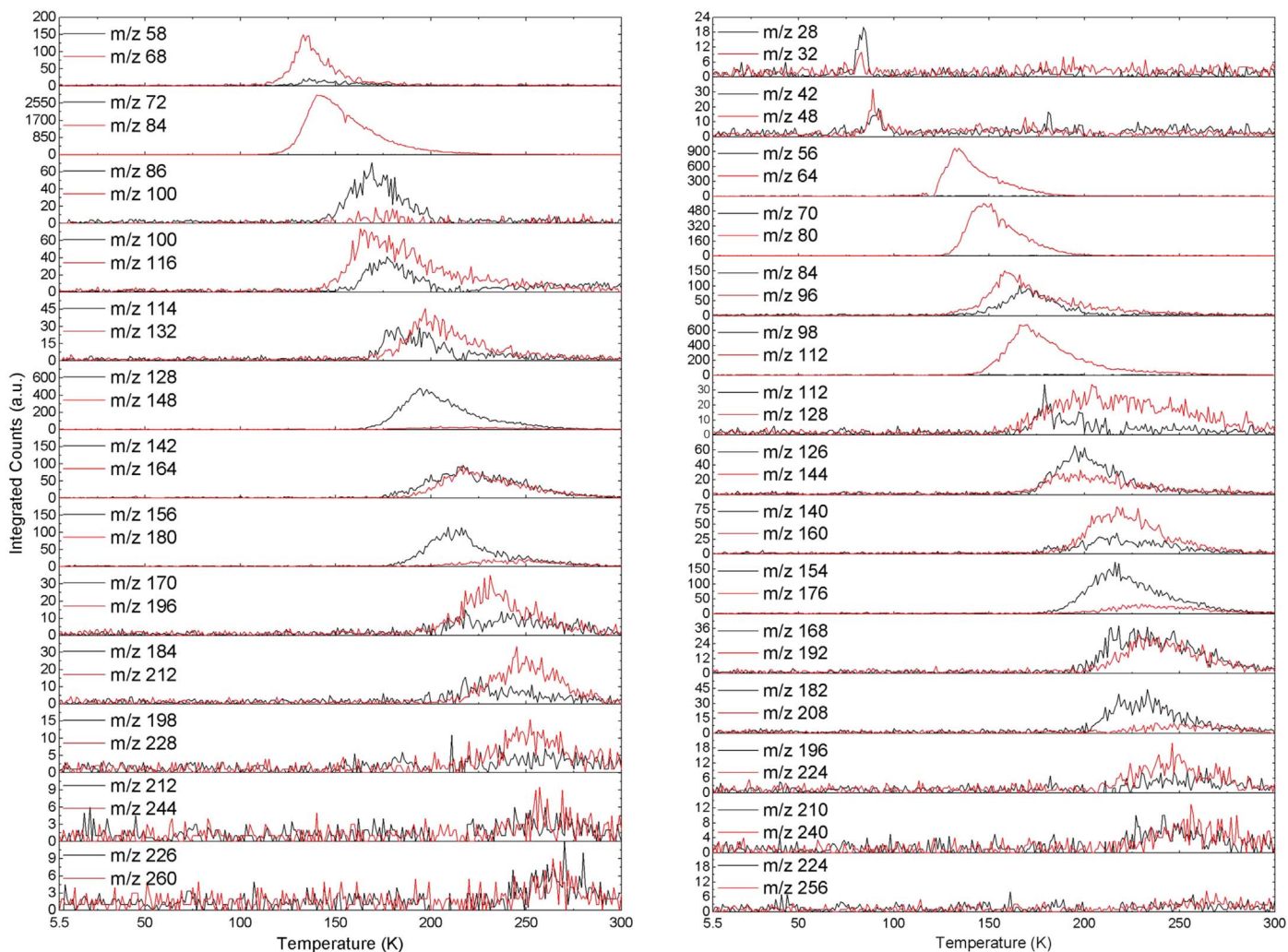


Figure 7. TPD profiles recorded after electron irradiation of C_2H_2 (black) and C_2D_2 (red) via PI-ReTOF-MS for masses with the generic formula of C_nH_{2n+2}/C_nD_{2n+2} (left) and C_nH_{2n}/C_nD_{2n} (right).

because the only other isomer, i-butane, has a photoionization energy of 10.68 ± 0.11 (Lias et al.), which will not be ionized and therefore not detected. The isomer-specific detection of n-butane demonstrates how individual isomers are able to be detected utilizing tunable photoionization. Note that all ionization energies in the current and following sections correspond to gas-phase ionization values.

Also, the general molecular formulae are observed to grow by an additional CH_2 unit to the next-largest alkane, except for $n = 5$, but an interesting trend that the product ion signals differ between the two acetylene systems (C_2H_2/C_2D_2) suggests that highly unsaturated hydrocarbons, which have overlapping mass-to-charge ratios, may also be produced. This difference is apparent in the shape of the sublimation profile, as well as the complete absence in some cases of the isotopologue ion signal, and if only alkanes were produced, the signals of the isotopologues should be identical. However, alkanes cannot be ruled out completely without further experiments, and some are definitely produced, as both ethane and n-butane were able to be confirmed as products.

Interestingly, most previous experiments utilizing ionizing radiation do not report any alkanes as products (Floyd et al. 1973; Strazzulla et al. 2002; Wu & Cheng 2008; Zhou et al. 2010;

Cuyllé et al. 2014; Ryazantsev et al. 2018), and the experiments that did record alkane products detected them only from $n = 1-11$ (Kaiser & Roessler 1998). While alkanes have not been detected in the interstellar medium (ISM), ethane and propane have both been detected on Saturn and Titan, and ethane has also been detected on Jupiter, Uranus, and Neptune, as well as on several comets. Also, alkanes have been a commonly detected group in meteorite analysis (Gelpi & Oró 1970; Sephton et al. 2001).

4.3. C_nH_{2n}

The next hydrocarbon group of discussion corresponds to alkenes (C_nH_{2n}) and/or cycloalkanes of $n = 2, 3, 6, 8-16$ (Figure 7). Although only ethylene was able to be assigned via FTIR, numerous other alkenes, or cycloalkanes, were also produced. The nondetection of alkenes with carbon chains of $n = 4, 5$, and 7 may be important in understanding the reaction mechanism to produce the products of acetylene irradiation, and the ion signal present for their isotopologue only reaffirms that highly unsaturated hydrocarbons are preferentially formed, as these have mass-to-charge ratios that overlap with the alkene group. For example, Zhou et al. (2014) showed that

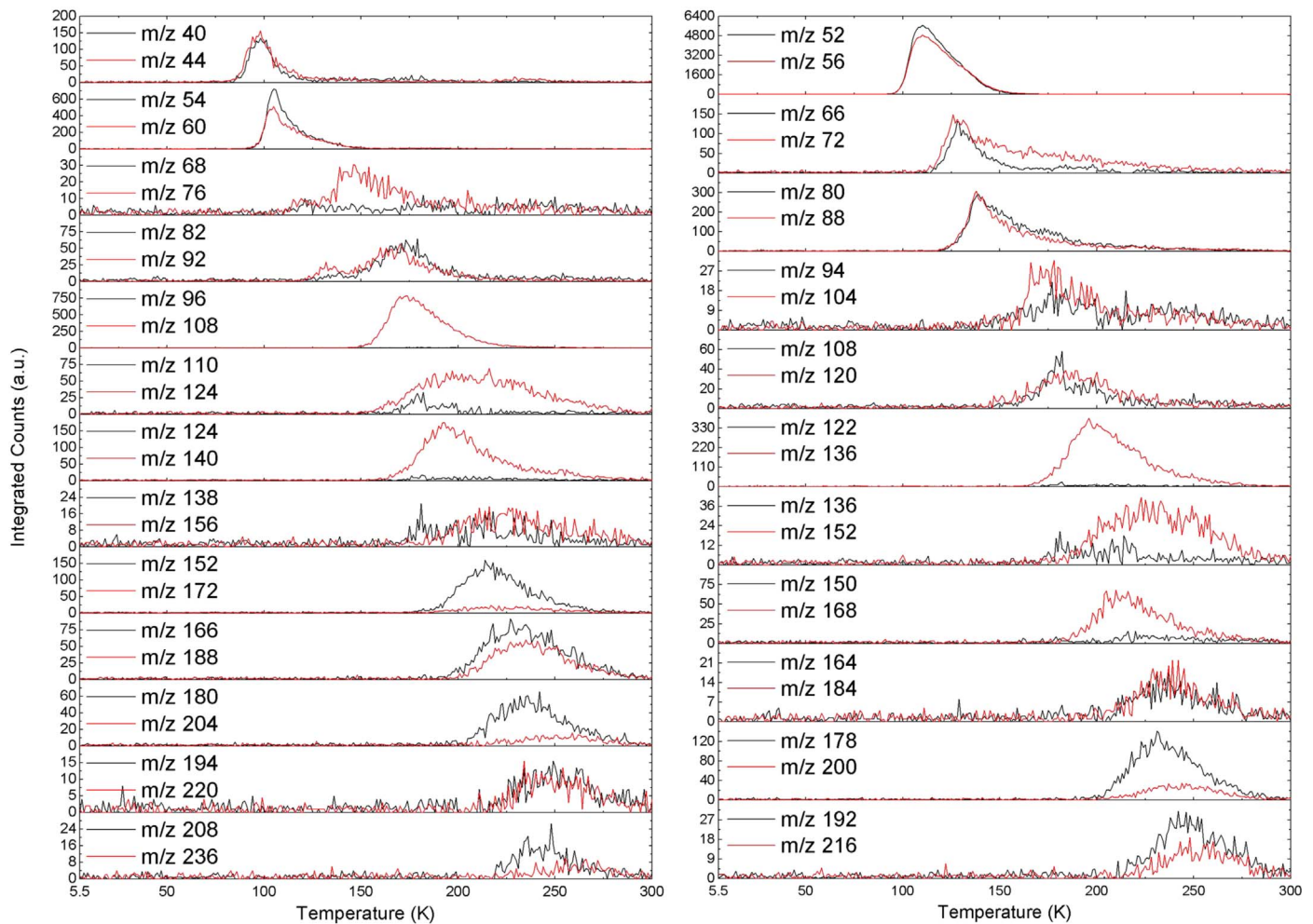


Figure 8. TPD profiles recorded after electron irradiation of C_2H_2 (black) and C_2D_2 (red) via PI-ReTOF-MS for masses with the generic formula of C_nH_{2n-2}/C_nD_{2n-2} (left) and C_nH_{2n-4}/C_nD_{2n-4} (right).

radiolysis of n-butane converts it to 1-butene, an alkene, but the ion signal for butene was not detected, although butane was confirmed.

Again, most previous experiments processing acetylene ices with ionizing radiation did not detect any alkenes/cycloalkanes as products (Floyd et al. 1973; Strazzulla et al. 2002; Wu & Cheng 2008; Zhou et al. 2010; Cuyllé et al. 2014; Ryazantsev et al. 2018), and the studies that did detect this group only observed ethylene (C_2H_4), cyclopropane ($c-C_3H_6$), and propene (C_3H_6) (Kaiser & Roessler 1998). The detection of C_3H_6 ($m/z = 42$), which can only be propylene (CH_2CHCH_3 ; I.E. = 9.73 eV) or cyclopropane (I.E. = 9.86 eV), is very interesting, as propylene has been detected in the ISM (Marcelino et al. 2007) and its astrophysical formation route has been investigated (Lin et al. 2013; Rawlings et al. 2013; Abplanalp et al. 2018b). Meanwhile, the cyclopropane isomer is the simplest possible cyclic alkane that can be produced. Either of these isomers may be responsible for the ion signal detected at 10.49 eV since both isomers are ionized if they were formed. It has been shown that propylene (CH_2CHCH_3) reacts with carbon atoms (C ; 3P_j) (Kaiser et al. 1997), along with dicarbon molecules (C_2) (Dangi et al. 2013), via crossed molecular beams experiments, to produce the PAH precursors methylpropargyl radical (C_4H_5), as well as 1- and 3-vinylpropargyl, respectively. Also, theoretical models designed to understand

Titan’s atmosphere utilized several alkenes ($n = 2-6$) to replicate gas-phase reactions possibly taking place, revealing that there is a tendency to produce multiple unsaturated bonds upon exposure to ionizing radiation (Woon & Park 2009). Further, the UV processing of PAHs with cyclodecane ($C_{10}H_{20}$) under ISM conditions revealed that photoalkylation is possible.

4.4. C_nH_{2n-2}

SPI-ReTOF-MS also identified ion signals corresponding to alkynes (C_nH_{2n-2}), dienes, cycloalkenes, and/or bicycloalkanes with $n = 3, 4, 6, 8, 10-15$ (Figure 8). The FTIR analysis did not reveal any products in this hydrocarbon group, but the SPI-ReTOF-MS showed numerous alkyne type ions present. Here, the undetected carbon chains ($n = 5, 7, 9$) corresponded only to odd-valued lengths, which may provide insight into the formation pathway of the acetylene irradiation products.

Even alkynes, dienes, cycloalkenes, and/or bicycloalkanes remained elusive to several previous studies as a product of irradiated acetylene ice (Floyd et al. 1973; Strazzulla et al. 2002; Wu & Cheng 2008; Zhou et al. 2010; Cuyllé et al. 2014; Ryazantsev et al. 2018), but the group was detected in a single study via allene (C_3H_4) and methylacetylene (C_3H_4) (Kaiser & Roessler 1998). The ion signal detected for $m/z = 40$ (C_3H_4)

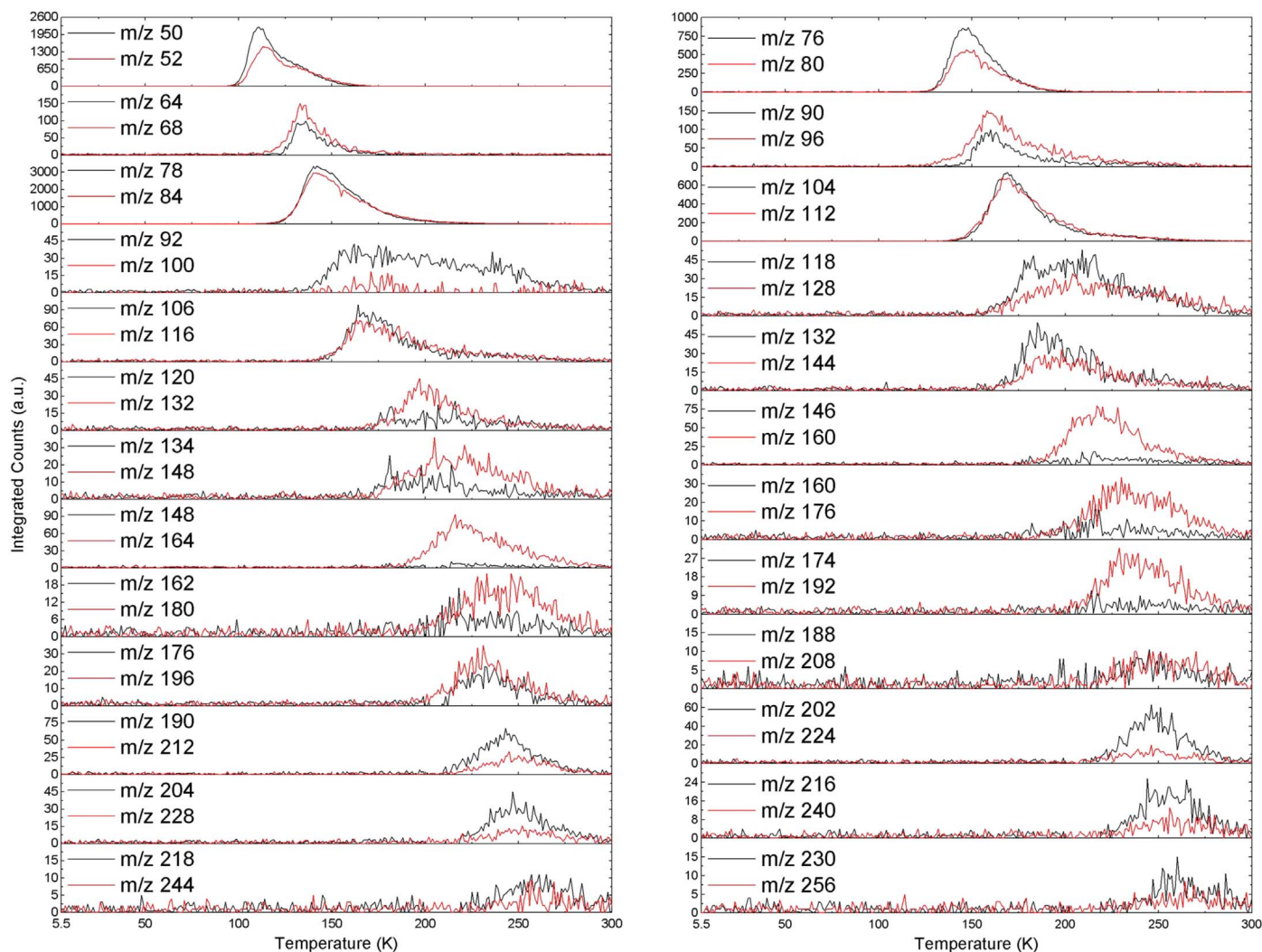


Figure 9. TPD profiles recorded after electron irradiation of C_2H_2 (black) and C_2D_2 (red) via PI-ReTOF-MS for masses with the generic formula of C_nH_{2n-6}/C_nD_{2n-6} (left) and C_nH_{2n-8}/C_nD_{2n-8} (right).

can belong to either methylacetylene (CH_3CCH ; IE = 10.36 eV) or its isomer allene (H_2CCCH_2 ; IE = 9.69 eV). The methylacetylene isomer was detected in several surveys toward Sgr B2, PKS 1830–211, L1544, and tentatively in NCG 4418 (Belloche et al. 2013; Muller et al. 2014; Vastel et al. 2014; Costagliola et al. 2015). Methylacetylene and allene have both been reactants used to untangle the chemistry taking place in Titan’s atmosphere (Vakhtin et al. 2001; Goulay et al. 2007; Zhang et al. 2009a). Several experiments have elucidated that allene and methylacetylene are both very important for interstellar chemistry leading to PAH formation, as they are shown to react with the phenyl radical (C_6H_5) to form indene (C_9H_8) (Parker et al. 2011, 2015b; Zhang et al. 2011a; Yang et al. 2015b).

Also, an ion signal corresponding to C_4H_6 was detected, which may be due to any of four isomers; these isomers are 1, 3-butadiene ($H_2CCHCHCH_2$; IE = 9.07 eV), 1, 2-butadiene ($H_2CCCH(CH_3)$; IE = 9.03 eV), 1-butyne ($HCCC_2H_5$; IE = 10.18 eV), and 2-butyne (CH_3CCCH_3 ; IE = 9.58 eV) (Lias et al.). The first isomer, 1, 3-butadiene, was revealed to be an extremely important molecule for PAH production in gas-phase reactions with dicarbon (C_2) to form the phenyl radical (C_6H_5) (Zhang et al. 2010), with the ethynyl radical (CCH)

producing benzene (C_6H_6) (Jones et al. 2011), as well as with the tolyl radicals ($C_6H_4CH_3$) synthesizing 6-methyl-1, 4-dihydronaphthalene ($C_{11}H_{12}$) (Parker et al. 2014b). Dartois et al. (2005) photolyzed solid 1, 5–hexadiene (C_6H_{10}) with UV photons that formed a carbonaceous polymer. Also, Stephens & Bauer (1994) have investigated the infrared emissions of 2, 4-dimethyl-1, 3-pentadiene (C_7H_{12}), among other hydrocarbons, through shock heating to resolve their possible influence in ISM PAH signatures.

4.5. C_nH_{2n-4}

The hydrocarbon group associated with yne-enes, trienes, cyclodialkenes, and bicycloalkenes, having the general formula C_nH_{2n-4} ($n = 4-8, 10-14$), was detected via SPI-ReTOF-MS (Figure 8). Although no FTIR detection of the previous group was possible, the simplest of this group, C_4H_4 , was observed via FTIR analysis by detection of vinylacetylene ($CHCCHCH_2$). The ion signal corresponding to C_4H_4 was observed to be the most intense signal detected, but further tunable experiments are necessary to elucidate which isomer(s) this signal belongs to in order to quantify its yield. For this hydrocarbon group only the carbon chain corresponding to $n = 9$ could not be detected, while $n = 4-8$ and $10-14$ are at

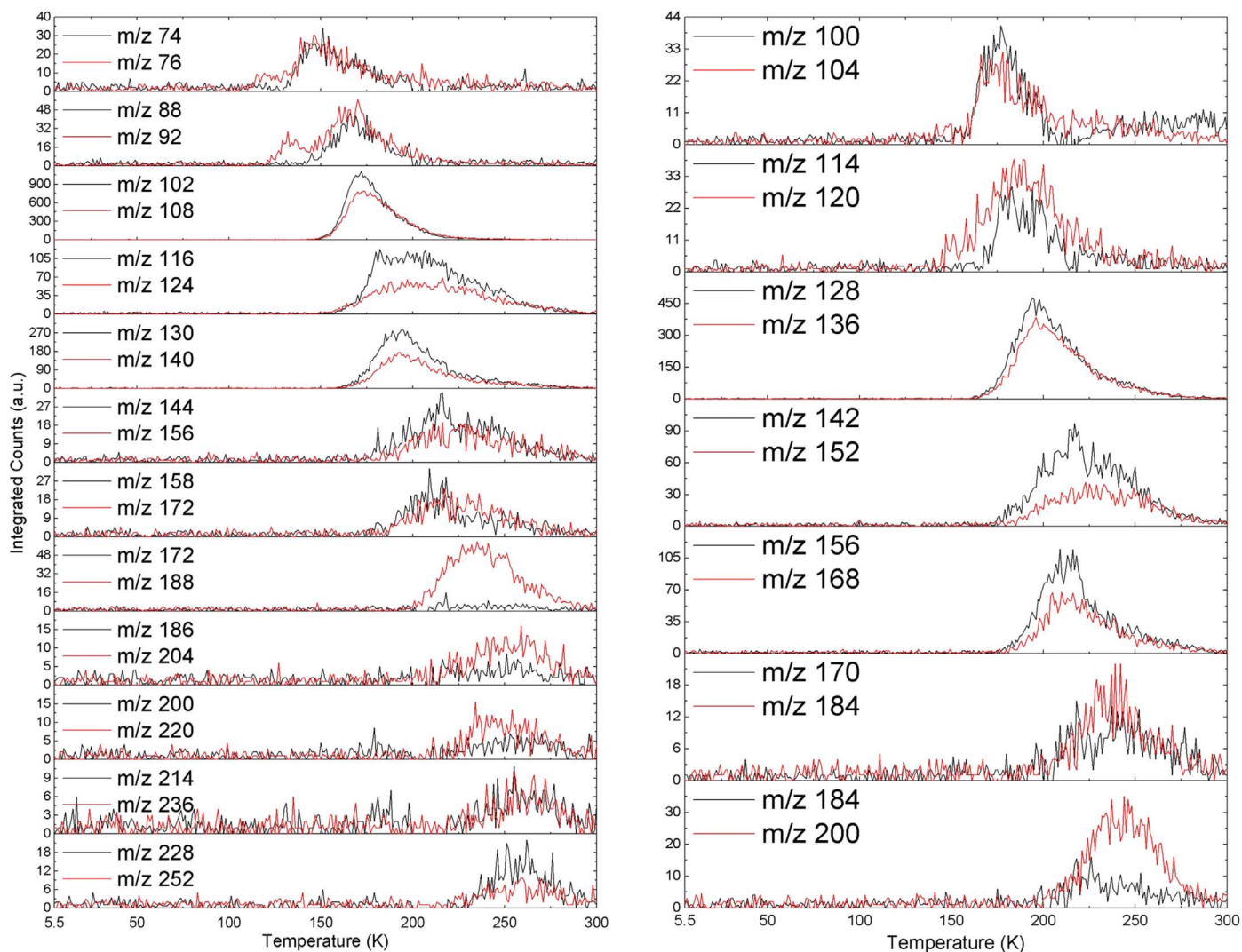


Figure 10. TPD profiles recorded after electron irradiation of C_2H_2 (black) and C_2D_2 (red) via PI-ReTOF-MS for masses with the generic formula of $C_nH_{2n-10}/C_nD_{2n-10}$ (left) and $C_nH_{2n-12}/C_nD_{2n-12}$ (right).

least minor contributors to the corresponding ion signal in all cases and major contributors for a few signals.

Several previous experiments have observed this hydrocarbon group via C_4H_4 assigned to vinylacetylene (Floyd et al. 1973; Ryazantsev et al. 2018), as well as its isomer methylenecyclopropene (Zhou et al. 2010). As noted above, this group contained an ion signal $m/z = 52$ (C_4H_4), which may be due to the astrophysically important isomer vinylacetylene ($CHCCHCH_2$; I.E. = 9.58 eV) associated with it (Lias et al.). Vinylacetylene has been investigated multiple times and determined to be important for Titan’s chemistry (Kim & Kaiser 2009; Zhang et al. 2009c; Vuitton et al. 2012) and to produce prototype PAHs such as naphthalene ($C_{10}H_8$) (Parker et al. 2012), 2-methylnaphthalene ($C_{11}H_{10}$) (Parker et al. 2014a), and 1-methylnaphthalene ($C_{11}H_{10}$) in the gas phase (Yang et al. 2015a).

4.6. C_nH_{2n-6}

In addition, the hydrocarbon group C_nH_{2n-6} ($n = 4-10$, 12–16) was detected as a product of acetylene irradiation (Figure 9). Here, the simplest hydrocarbon in this group,

diacetylene (C_4H_2), was confirmed via FTIR (Tables 1, 2), and as this molecule has no other isomers, its ion signal can be used to determine its yield. Similar to the last group, a single odd carbon chain molecule ($n = 11$) was the only nondetection from $n = 4-16$, while all other ion signals between the isotopologues match well. As stated earlier, several of these ion signals may have multiple contributors or a single more highly unsaturated identity. For example, the deuterated ion signal at $m/z = 84$ may only be due to C_5D_{12} or C_6D_6 , and upon comparing this ion signal to C_5H_{12} ($m/z = 72$) and C_6H_6 ($m/z = 78$), the alkane can be ruled out and the C_6H_6/C_6D_6 molecule was confirmed. This detection is very interesting, as one isomer belonging to C_6H_6 is benzene, a hydrocarbon constructed as an aromatic ring, which is often discussed as a prototypical PAH.

This group was detected in prior acetylene irradiation experiments by observation of diacetylene (C_4H_2) (Floyd et al. 1973; Cuyllé et al. 2014; Ryazantsev et al. 2018) and C_6H_6 , which may possibly be the benzene isomer (Zhou et al. 2010; Cuyllé et al. 2014). Both diacetylene (C_4H_2) and benzene ($c-C_6H_6$), which have both been identified here, are also detected in Titan’s atmosphere (Coustenis et al. 2003, 2007), as well as in

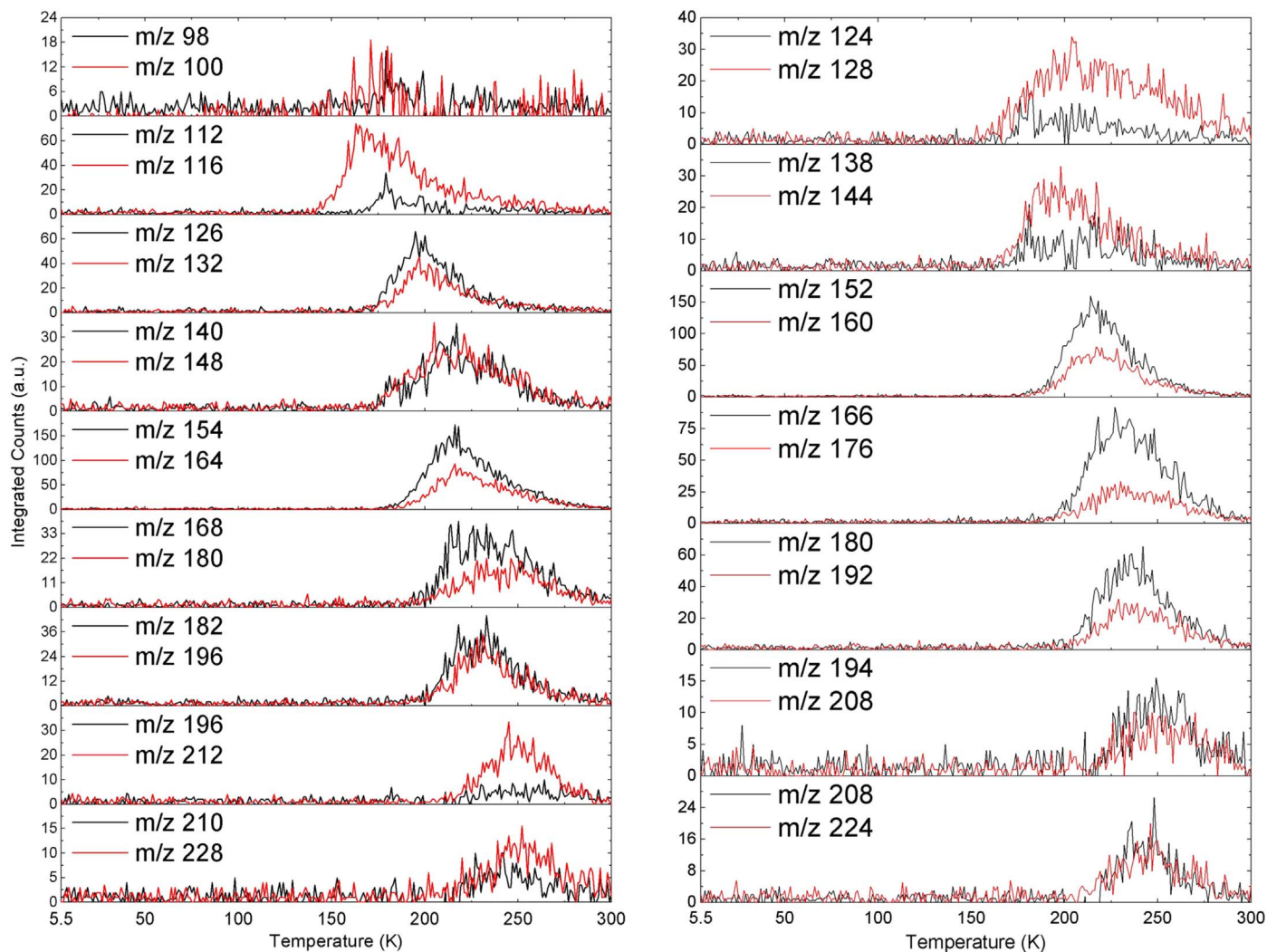


Figure 11. TPD profiles recorded after electron irradiation of C_2H_2 (black) and C_2D_2 (red) via PI-ReTOF-MS for masses with the generic formula of $C_nH_{2n-14}/C_nD_{2n-14}$ (left) and $C_nH_{2n-16}/C_nD_{2n-16}$ (right).

other atmospheres and even in the ISM (Bézar et al. 2001; Cernicharo et al. 2001; Burgdorf et al. 2006; Guerlet et al. 2010). Another molecule belonging to this group, methyl diacetylene (C_5H_4), has also been detected in the ISM in TMC-1 (Loren et al. 1984; MacLeod et al. 1984; Walmsley et al. 1984). Diacetylene was shown to react with dicarbon in the gas phase and produce the PAH precursor 1, 3, 5-hexatriynyl radical (Zhang et al. 2009b). Sivaraman et al. (2015) irradiated propargyl alcohol, which produced benzene as a major product, supporting that this molecule can be synthesized in the ice. Jones et al. (2011) revealed that benzene is capable of forming via the reaction of the ethynyl radical and 1, 3-butadiene in the gas phase. Benzene may then undergo further reactions that have also been studied in the gas phase with carbon atoms (Bettinger et al. 2000; Kaiser et al. 2003), dicarbon (Gu et al. 2007b), tricarbon molecules (Gu et al. 2007a), and phenyl radicals (C_6H_5) (Zhang et al. 2008), producing 1, 2-didehydrocycloheptatrienyl radical (C_7H_5), phenylethynyl radical (C_6H_5CC), phenyltricarbon (C_6H_5CCC), and diphenyl ($C_6H_5C_6H_5$), respectively. Finally, Gudipati & Yang (2012) showed that toluene (C_7H_8), also in this hydrocarbon group, undergoes hydroxylation when present in astrophysical ice analogs.

4.7. C_nH_{2n-8}

Another product group, C_nH_{2n-8} ($n = 6-10, 12, 14-17$), was also detected with SPI-ReTOF-MS (Figure 9). Although no FTIR detections for this group were confirmed, the SPI-ReTOF-MS data revealed numerous ion signals produced corresponding to this unsaturated group. Carbon chains ranging from $n = 6$ to 17 were detected, but $n = 11$ and 13 remained undetected, which is similar to several of the previously discussed groups and may help to elucidate the formation pathway to these products.

No previous studies of acetylene irradiation products detected this hydrocarbon group (Floyd et al. 1973; Kaiser & Roessler 1997, 1998; Strazzulla et al. 2002; Wu & Cheng 2008; Zhou et al. 2010; Cuyllé et al. 2014; Ryazantsev et al. 2018). Interestingly, theoretical studies have been carried out to understand the formation pathways to different C_6H_4 isomers, which correspond to the smallest hydrocarbon detected for this group in the present experiment, from acetylene (Bera et al. 2015). Also, the ortho-benzyne (*o*- C_6H_4) isomer was detected as a product from the reaction of vinylacetylene and the ethynyl radical in the gas phase (Zhang et al. 2011b). Fulvenallene (C_7H_6) is another important molecule from this group that was

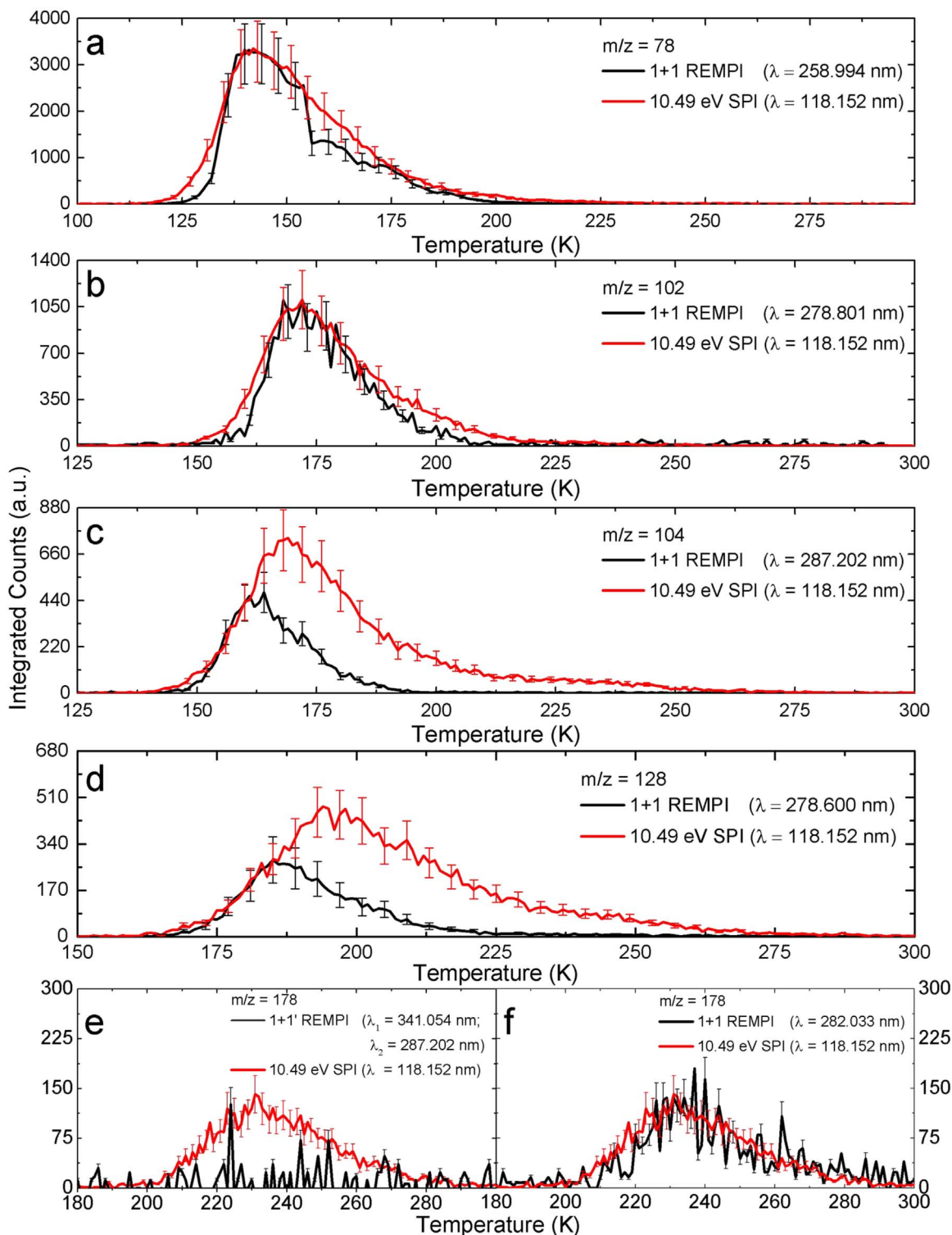


Figure 12. Overlay of REMPI (black) and SPI (red) ion signals vs. temperature for (a) $m/z = 78$ (benzene), (b) $m/z = 102$ (phenylacetylene), (c) $m/z = 104$ (styrene), (d) $m/z = 128$ (naphthalene), and (e, f) $m/z = 178$ (phenanthrene).

reacted with both atomic carbon (da Silva 2014) and the hydroxyl radical (Thapa et al. 2015) to investigate the fulvenallenyl radical, a precursor to PAHs. Styrene ($C_6H_5C_2H_3$) reacting with ethynyl radicals was also studied to investigate PAH growth pathways (Landera et al. 2011), and styrene was confirmed as a product from the gas-phase bimolecular reaction of ethylene and phenyl radicals (Zhang et al. 2007).

4.8. C_nH_{2n-10}

SPI-ReTOF-MS also confirmed the presence of the hydrocarbon group C_nH_{2n-10} ($n = 6-12, 14-17$) (Figure 10). No specific molecule corresponding to this group was able to be detected through FTIR analysis, but numerous ion signals corresponding to carbon chain lengths from $n = 6$ to 17 were detected, except at $n = 13$. Again, the only nondetected ion

signal in this group was for an odd carbon chain length, which is a trend seen in most of the groups discussed so far and suggests a reaction mechanism preferentially leading to even-valued carbon chains for the products. All of the detected ion signals for this group ($n = 6-12, 14-17$) match their deuterated isotopologue signal very well. Here, the signal at $m/z = 74$ corresponds to 1, 3, 5-hexatriene (C_6H_2), which is the only isomer for this group, but all other signals have several isomeric possibilities, and additional tunable experiments are needed to elucidate their identities.

Floyd et al. (1973) detected this highly unsaturated group via an ion signal corresponding to C_8D_6 but could not identify a specific isomer. This group has several molecules associated with it that have been detected and/or studied by the astrochemistry community. For example, 1, 3, 5-hexatriene (C_6H_2) was observed in CRL 618 (Fonfría et al. 2011), and methyltriacetylene (C_7H_4) was also observed toward TMC-1 (Remijan et al. 2006). Both 1, 3, 5-hexatriene (C_6H_2) and phenylacetylene (C_8H_6) have been shown to form over forsterite and olivine samples through an aromatization reaction of acetylene (Tian et al. 2012). Also, phenylacetylene (C_8H_6) was shown to be the product of the bimolecular reaction of the phenyl radical with acetylene (Xibin Gu et al. 2007), as well as between the ethynyl radical and benzene (Jones et al. 2010). A computational study investigating the formation pathways to C_6H_2 isomers from acetylene and its fragments has also been conducted (Bera et al. 2015). It was recently shown that the pentalene isomer (C_8H_6) may be synthesized through dissociative ionization of naphthalene (Bouwman et al. 2016).

4.9. C_nH_{2n-12}

Also detected via SPI-ReTOF-MS in the present study was C_nH_{2n-12} ($n = 8-14$) (Figure 10). This hydrocarbon group was only detected through the more sensitive SPI-ReTOF-MS technique. Here, all ion signals were detected from $n = 8-14$ and confirmed with their deuterium isotopologues, which is a different trend from the previous groups discussed so far. While there could be other contributors to these ion signals, the C_nH_{2n-12} ($n = 8-14$) molecules are at least partially responsible for the signal and likely to be major contributors for carbon chains of $n = 8-13$.

This group was previously detected via an ion signal corresponding to $C_{10}D_8$ (Floyd et al. 1973). This group contains the simplest PAH constructed with two fused benzene rings, naphthalene ($C_{10}H_8$), which has been used to unravel the identity of diffuse interstellar bands (DIBs; Pauzat et al. 1995; Beegle et al. 1997; Pauzat & Ellinger 2001; Yang et al. 2013). Naphthalene has been shown to form over forsterite and olivine samples through an aromatization reaction of acetylene (Tian et al. 2012). The closely related molecules 1- and 2-methylnaphthalene ($C_{11}H_{10}$), whose corresponding mass-to-charge ratio has been detected in this experiment, have been shown to form via bimolecular collisions in the gas phase and are also a possible carrier of the DIBs (Yang et al. 2015a).

4.10. C_nH_{2n-14}

Next, detected via SPI-ReTOF-MS was the C_nH_{2n-14} ($n = 8-16$) (Figure 11) hydrocarbon group. Again the sensitive SPI-ReTOF-MS technique revealed this group, while it remained elusive to FTIR detection. Like the previous group, the ion signals from $n = 8-16$ were all detected, with none

missing in this range, which supports that highly unsaturated products are easily formed from the irradiated acetylene ice. Like several of the previous hydrocarbon groups, the present experiment is the first to detect the C_nH_{2n-14} group.

The simplest molecule detected in this hydrocarbon group, 1, 3, 5, 7-octatetrayne (C_8H_2), or tetraacetylene, has been detected in the ISM in CRL 618 (Fonfría et al. 2011) and has been proposed as a possible contributor to the DIBs (Doney et al. 2018). Tetraacetylene has also been shown to form the reaction of the hexatrienyl radical (C_6H), which has been detected in TMC-1, and acetylene (Sun et al. 2015). Another astrophysically important molecule, whose ion signal was detected here, is phenyldiacetylene ($C_{10}H_6$), which can be formed from the reaction of phenylethynyl radical (C_6H_5CC) and acetylene, or the ethynyl radical (C_2H) and phenylacetylene ($C_6H_5C_2H$); the latter reaction also produces 1, 2-diethynylbenzene ($C_{10}H_6$) (Mebel et al. 2008). Another isomer, Didehydronaphthalene, has also been used to investigate DIBs' correspondence to PAH-type molecules (Pauzat et al. 1995). Also, another $C_{10}H_6$ isomer, 1, 3-diethynylbenzene, along with 3-ethynylindene ($C_{11}H_8$), has been proven to form from acetylene aromatization via forsterite and olivine samples (Tian et al. 2012). The ion signal corresponding to $C_{12}H_{10}$ detected here also belongs to an astrophysically important group of isomers, as biphenyl was detected in both the Murchison and Orgueil meteorites (Callahan et al. 2013), and acenaphthene has been previously used to scrutinize the DIBs (Halasinski et al. 2005).

4.11. C_nH_{2n-16}

Finally, the most highly unsaturated group detected via SPI-ReTOF-MS in the present study was C_nH_{2n-16} ($n = 10-16$) (Figure 11). Continuing the trend of the previous few groups, all ion signals from $n = 10-16$ were detected with no discontinuity, further suggesting that acetylene irradiation results in the facile production of highly unsaturated hydrocarbons. No previous studies were able to detect this highly unsaturated group.

The ion signal detected at $m/z = 152$ may correspond to the astrophysically important molecule, acenaphthylene ($C_{12}H_8$), which can form from the aromatization of acetylene interacting with forsterite and olivine samples (Tian et al. 2012) and can also be synthesized in the gas phase via the barrierless bimolecular reaction of the naphthyl radical ($C_{11}H_7$) with acetylene (Parker et al. 2015a). Acenaphthylene ($C_{12}H_8$) and fluorene ($C_{13}H_{10}$), along with 9, 10-dihydroanthracene ($C_{14}H_{12}$) and 9, 10-dihydrophenanthrene ($C_{14}H_{12}$), have also been studied to explain the identity of the DIBs (Allamandola et al. 1999; Mallocci et al. 2004, 2007; Mulas et al. 2006; Pathak et al. 2014; Ota 2017; Mackie et al. 2018). Another possible molecule detected in the present experiment, the 1, 4-dihydrophenanthrene ($C_{14}H_{12}$) molecule, has previously been proven to form from the bimolecular reaction of 1-naphthyl radical ($C_{11}H_7$) with 1, 3-butadiene (C_4H_6) in the gas phase (Thomas et al. 2017).

4.12. REMPI-ReTOF-MS

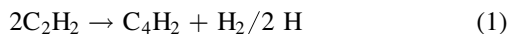
The similarity of the SPI and REMPI-ReTOF-MS TPD profiles recorded at $m/z = 78$ ($C_6H_6^+$) and 102 ($C_8H_6^+$) exposed that both benzene and phenylacetylene are the major constituents of their respective ion signal (Figures 12(a) and (b));

Swenson & Gillispie 1996; Tzeng et al. 1999). The minor discrepancies between the SPI and REMPI sublimation profiles for $m/z = 78$ and 102 are due to the ionization of additional C_6H_6 and C_8H_6 isomers via SPI at 10.49 eV that cannot be ionized through REMPI. The REMPI experiments also detected styrene (C_8H_8) and naphthalene ($C_{10}H_8$), and a detailed analysis of the SPI and REMPI data revealed that these isomers are only responsible for a portion of the ion signal. Since the SPI and REMPI data only correspond well with each other at the low temperatures of 140–200 K and 160–260 K for styrene and naphthalene, respectively, other isomers must contribute to these ion signals (Figures 12(c) and (d)). The detection of $m/z = 178$ ($C_{14}H_{10}^+$) via both one- and two-color REMPI schemes ($\lambda_1 = 341.054 \pm 0.001$ nm, 3.635 eV; $\lambda_2 = 287.202 \pm 0.001$ nm, 4.317 eV) confirmed the formation of phenanthrene (Figures 12(d) and (f)). Here, the two-color REMPI scheme was used for isomer-specific detection of phenanthrene, while the one-color process produces a stronger signal (Klimcak & Wessel 1980; Hager & Wallace 1988). Note that larger PAHs were also ionized and detected utilizing REMPI owing to their broad absorptions in this region (Abplanalp et al. 2019).

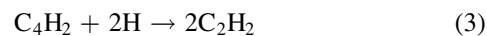
These aromatic hydrocarbons have been studied numerous times in an astrophysical context. Bimolecular gas-phase reactions with benzene and carbon atoms (Bettinger et al. 2000; Kaiser et al. 2003), dicarbon (Gu et al. 2007b), tricarbon molecules (Gu et al. 2007a), and phenyl radicals (C_6H_5) (Zhang et al. 2008) produced 1, 2-didehydrocycloheptatrienyl radical (C_7H_5), phenylethynyl radical (C_6H_5CC), phenyltricarbon (C_6H_5CCC), and diphenyl ($C_6H_5C_6H_5$), respectively. Similarly, phenylacetylene (C_8H_6) was a detected product of the phenyl radical reacting with acetylene (Xibin Gu et al. 2007), as well as between the ethynyl radical and benzene (Jones et al. 2010), and phenylacetylene itself was shown to react with the cyano radical (CN) to form cyanophenylacetylene (C_8H_5CN). Styrene ($C_6H_5C_2H_3$) has previously been shown to react with ethynyl radicals to investigate PAH growth pathways (Landra et al. 2011) and is a product from the bimolecular reaction of ethylene and phenyl radicals (Zhang et al. 2007). Naphthalene, a prototype PAH consisting of two fused benzene rings, has been produced via bimolecular gas-phase reactions between vinylacetylene and the phenyl radical (Parker et al. 2012). Finally, phenanthrene has been synthesized through bimolecular gas-phase reactions of the biphenyl radical ($C_{12}H_9$) and acetylene (Yang et al. 2017).

4.13. Reaction Mechanism and Carbon Budget

The detection of ethane (C_2H_6/C_2D_6), ethylene (C_2H_4/C_2D_4), diacetylene (C_4H_2/C_4D_2), vinylacetylene (C_4H_4/C_4D_4), and benzene (C_6H_6/C_6D_6) via infrared spectroscopy permits the kinetic fitting of each product's column density (molecules cm^{-2}) via the numerical solving of coupled differential equations (Figure 13). The reaction pathways utilized in solving the kinetic fits are shown in Figure 14, and the corresponding rate constants are listed in Table 4. This set of coupled chemical equations provided the best fit to experimental data. By kinetically fitting the experimental data, acetylene is shown to undergo successive reactions with neighboring acetylene molecules to synthesize more complex hydrocarbons such as diacetylene (reaction (1)) and vinylacetylene (reaction (2)):



Here, in case of ground-state reactants, reaction (1) is energetically unfavorable with an endoergicity of 8 kJ mol^{-1} , but reaction (2) is exoergic by -161 kJ mol^{-1} . Note that the reaction energies are calculated using gas-phase enthalpies. Additionally, the reaction of two acetylene molecules has a barrier of approximately 140 kJ mol^{-1} . This barrier will prevent either reaction from occurring under thermodynamic equilibrium at 5 K on the ground state surface, and therefore these reactions must involve nonequilibrium routes that provide enough energy to overcome this reaction barrier. However, the secondary electrons penetrating through the ice can transfer part of their energy to the acetylene molecule(s), resulting in electronically excited acetylene, possibly in the a^3B_2 , b^3B_u , or c^3A_u states, which were calculated to lie 343, 372 and 407 kJ mol^{-1} above ground-state acetylene, respectively (Ventura et al. 2003). These excited states represent the lowest electronically excited acetylene states, yet they provide enough to overcome the barrier of 140 kJ mol^{-1} and allow the reaction to proceed even at low temperatures of 5 K. Similar mechanisms utilizing electronically excited acetylene (Zhou et al. 2008) and ethylene (Abplanalp et al. 2015) were observed in the reactions with carbon monoxide (CO), leading to cyclopropenone (C_2H_2CO) and cyclopropanone (C_2H_4CO), respectively. The kinetic fitting also revealed that both reaction (1) and reaction (2) are reversible, as diacetylene can react with suprathreshold hydrogens and decompose into two acetylene molecules (reaction (3)) and vinylacetylene can decompose into two acetylene molecules (reaction (4)):



Alternatively, vinylacetylene may react with another acetylene molecule to produce benzene (reaction (5)). However, Zhou et al. (2010) showed that three acetylene molecules may react successively to form benzene as well (reaction (6)). Although both reactions (5) and (6) are highly exoergic by -422 and -583 kJ mol^{-1} , respectively, they are hindered by an entrance barrier. The initial step in reaction (6) has an approximate reaction barrier of 140 kJ mol^{-1} , which blocks the reaction sequence involving two acetylene molecules on the singlet surface, leading to C_4H_4 reaction intermediates (Zhou et al. 2010). As previously stated, nonequilibrium processes such as via excited acetylene must therefore be responsible for allowing the reaction to take place. Electronically excited triplet acetylene (a^3B_2) reacting with an adjacent acetylene molecule has a considerably smaller barrier of 4 kJ mol^{-1} , which can be easily overcome via vibrational energy of a reactant, forming an acyclic triplet C_4H_4 intermediate (Zhou et al. 2010). The triplet C_4H_4 intermediate can then react with another acetylene molecule producing triplet benzene that will undergo intersystem crossing to singlet benzene. The benzene molecule is a suggested starting point for more complex hydrocarbons (X) such as PAHs; the kinetic fit shows that this buildup takes place in further reactions, which are likely the mass growth processes to more complex species (reaction (7)):



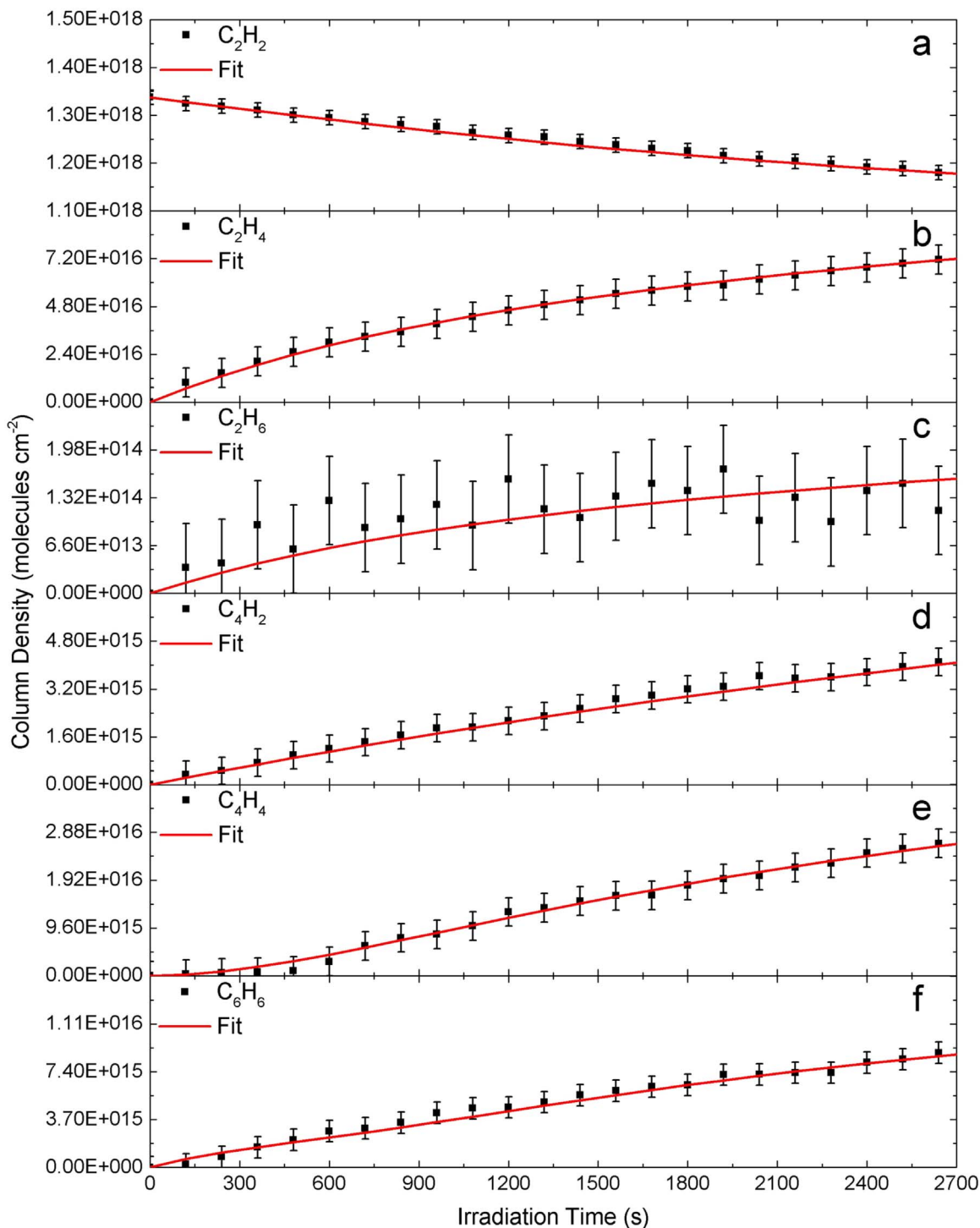


Figure 13. Temporal evolution and kinetic fitting of (a) acetylene, (b) ethylene, (c) ethane, (d) diacetylene, (e) vinylacetylene, and (f) benzene. Rate constants derived from the kinetic fitting are compiled in Table 4.



Acetylene can also react with suprathermal hydrogen atoms—to overcome entrance barriers—to produce ethylene (reaction (8)), and ethylene can then be further hydrogenated by hydrogen atoms to produce ethane (reaction (9)). If the suprathermal hydrogen atoms can overcome the reaction barriers of reactions (9)–(10), these reactions will proceed

easily, as they are exoergic by -166 and -129 kJ mol^{-1} , respectively. Also, the ethylene product may also react with acetylene molecules to produce vinylacetylene, which is exoergic by -6 kJ mol^{-1} (reaction (10)). However, both ethane and ethylene also undergo decomposition to ethylene and acetylene, respectively (reactions (11)–(12)):

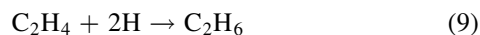
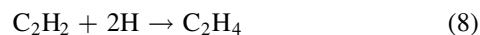


Table 4
Kinetic Fits

Reaction #	Chemical Reaction ^a	Rate Constant	Rate Constant Units
1	$C_2H_2 + C_2H_2 \rightarrow C_4H_2 + 2H$	$1.1 \pm 0.2 \times 10^{-24}$	$cm^2 \text{ molecules}^{-1} s^{-1}$
2	$C_2H_2 + C_2H_2 \rightarrow C_4H_4$	$1.0 \pm 0.2 \times 10^{-25}$	$cm^2 \text{ molecules}^{-1} s^{-1}$
3	$C_4H_2 + 2H \rightarrow C_2H_2 + C_2H_2$	$9.0 \pm 1.8 \times 10^{-5}$	$cm^4 \text{ molecules}^{-2} s^{-1}$
4	$C_4H_4 \rightarrow C_2H_2 + C_2H_2$	$9.9 \pm 2.0 \times 10^{-4}$	s^{-1}
5	$C_4H_4 + C_2H_2 \rightarrow C_6H_6$	$8.2 \pm 1.6 \times 10^{-22}$	$cm^2 \text{ molecules}^{-1} s^{-1}$
6	$C_2H_2 + C_2H_2 + C_2H_2 \rightarrow C_6H_6$	$2.8 \pm 0.6 \times 10^{-42}$	$cm^4 \text{ molecules}^{-2} s^{-1}$
7	$C_6H_6 \rightarrow X$	$3.2 \pm 0.6 \times 10^{-3}$	s^{-1}
8	$C_2H_2 + 2H \rightarrow C_2H_4$	$4.5 \pm 0.9 \times 10^{-5}$	$cm^4 \text{ molecules}^{-2} s^{-1}$
9	$C_2H_4 + 2H \rightarrow C_2H_6$	$9.9 \pm 2.0 \times 10^{-2}$	$cm^4 \text{ molecules}^{-2} s^{-1}$
10	$C_2H_2 + C_2H_4 \rightarrow C_4H_4 + 2H$	$4.9 \pm 1.0 \times 10^{-22}$	$cm^2 \text{ molecules}^{-1} s^{-1}$
11	$C_2H_6 \rightarrow C_2H_4 + 2H$	$4.5 \pm 0.9 \times 10^{+1}$	s^{-1}
12	$C_2H_4 \rightarrow C_2H_2 + 2H$	$3.8 \pm 0.8 \times 10^{-4}$	s^{-1}

Note.

^a The electronic states are not listed, as many states are accessible owing to the energetic electrons.

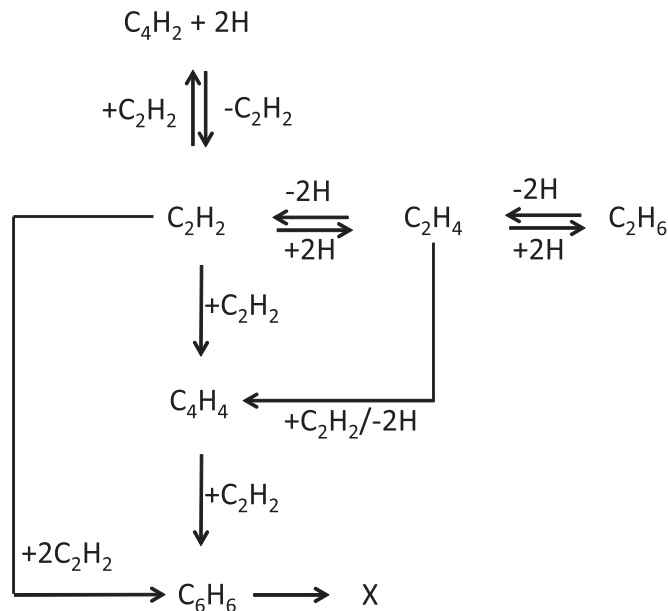
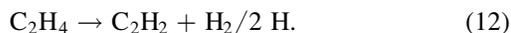
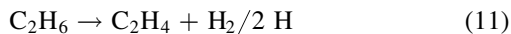


Figure 14. Chemical reaction scheme utilized in the coupled differential equation fitting for the column density of acetylene and the products of its radiolysis.



The carbon–hydrogen bond cleavage reaction to form an ethynyl radical (C_2H) and suprathermal hydrogen atom (reaction (13)) was not observed. Since only 3.1 eV (Table 3) was imparted into the acetylene ice on average, and this reaction needs about 5.7 eV to occur, this is justified as the reaction energy that can only be provided by the impinging electrons at the low temperature of the experiment (5 K). Although the ethynyl radical was not experimentally detected, it may have been generated via acetylene molecules that received an above-average dose and, if generated, may play a key role in polymerization reactions as they do in the gas

phase:



As stated above, benzene was observed to participate in further reactions, and with the REMPI detection of naphthalene and phenanthrene we propose that the addition of two additional acetylene molecules to benzene produces naphthalene, which then reacts again with two acetylene units synthesizing phenanthrene, as these reactions are exoergic by -405 kJ mol^{-1} and -404 kJ mol^{-1} , respectively (reactions (14)–(15)):



These reactions show that the pathways to major products involve increases in the carbon chain of two carbon atoms at a time, suggesting that the acetylene molecule does not break into individual carbon units, and this is also true for the other C2 hydrocarbons ethane and ethylene (Abplanalp & Kaiser 2016, 2017).

Furthermore, by monitoring the ice continuously, via FTIR during irradiation, temporal profiles for acetylene, ethylene, ethane, diacetylene, vinylacetylene, and benzene can be extracted (Figure 13). The FTIR temporal profile of acetylene shows that $(7.79 \pm 3.11) \times 10^{-2} \text{ molecules eV}^{-1}$ were consumed, which resulted in the products ethylene, ethane, diacetylene, vinylacetylene, and benzene being formed at $(3.47 \pm 1.39) \times 10^{-2} \text{ molecules eV}^{-1}$, $(6.51 \pm 2.60) \times 10^{-5} \text{ molecules eV}^{-1}$, $(2.01 \pm 0.81) \times 10^{-3} \text{ molecules eV}^{-1}$, $(1.38 \pm 0.62) \times 10^{-2} \text{ molecules eV}^{-1}$, and $(4.37 \pm 1.75) \times 10^{-3} \text{ molecules eV}^{-1}$, respectively (Table 5). The most abundant product at the end of irradiation was ethylene, which consumed $44.62\% \pm 17.85\%$ of the destroyed acetylene molecules, and the other C2 molecule, ethane, was the least abundant product, with a low abundance of $0.08\% \pm 0.03\%$ of the acetylene consumed in the experiment. The second and third most abundant products detected via FTIR were vinylacetylene and benzene, utilizing $17.67\% \pm 7.95\%$ and $5.62\% \pm 2.25\%$ of the reactant acetylene ice, respectively. Finally, the diacetylene molecule was also detected via FTIR and found to form from $2.58\% \pm 1.03\%$ of the acetylene molecules. The production of more vinylacetylene and benzene molecules compared to diacetylene molecules correlates well with the energetics discussed previously. Since

Table 5
Yields of Molecules Detected via FTIR

Species	Absorption Coefficient (cm molecules ⁻¹)	Yield (molecules eV ⁻¹)	% of Acetylene Consumed	References
Acetylene (C ₂ H ₂)	1388 cm ⁻¹ $2.33 \pm \times 10^{-18}$	$-7.79 \pm 3.11 \times 10^{-2}$...	1
Ethylene (C ₂ H ₄)	3095 cm ⁻¹ $1.51 \pm \times 10^{-18}$	$3.47 \pm 1.39 \times 10^{-2}$	44.62 ± 17.85	2
Ethane (C ₂ H ₆)	2887 cm ⁻¹ $3.81 \pm \times 10^{-18}$	$6.51 \pm 2.60 \times 10^{-5}$	0.08 ± 0.03	2
Diacetylene (C ₄ H ₂)	3328 cm ⁻¹ $3.3 \pm \times 10^{-17}$	$2.01 \pm 0.81 \times 10^{-3}$	2.58 ± 1.03	3
Vinylacetylene (C ₄ H ₄)	3280 cm ⁻¹ $1.3 \pm \times 10^{-17}$	$1.38 \pm 0.62 \times 10^{-2}$	17.67 ± 7.95	4
Benzene (C ₆ H ₆)	3030 cm ⁻¹ $2.86 \pm \times 10^{-18}$	$4.37 \pm 1.75 \times 10^{-3}$	5.62 ± 2.25	5
Total	70.57 ± 29.40	...

References. (1) Hudson et al. 2014b; (2) Hudson et al. 2014a; (3) Zhou et al. 2009a; (4) Kim & Kaiser 2009; (5) Yamada & Saheki 1983.

Table 6
Yields of Molecules Detected via PI-ReTOF-MS

Molecule	Formula	Adiabatic Ionization Energy (eV)	Photoionization Cross Section at 10.49 eV (Mb)	Yield (Molecules eV ⁻¹)	% of Acetylene Consumed	References
Diacetylene	C ₄ H ₂	10.17 ± 0.02	23.8 ± 4.8	$(2.66 \pm 0.93) \times 10^{-3}$	6.83 ± 2.39	1
Vinylacetylene	C ₄ H ₄	9.58 ± 0.02	32.5 ± 6.5	$^a(5.47 \pm 2.19) \times 10^{-3}$	14.04 ± 5.62	1
Benzene	C ₆ H ₆	9.244 ± 0.001	30 ± 6	$(3.72 \pm 1.28) \times 10^{-3}$	14.33 ± 5.01	1, 2, 3, 4, 5
Phenylacetylene	C ₈ H ₆	8.825 ± 0.001	63 ± 13	$(4.66 \pm 1.60) \times 10^{-4}$	2.39 ± 0.84	6
Styrene	C ₈ H ₈	8.464 ± 0.001	40 ± 8	$(2.74 \pm 0.94) \times 10^{-4}$	1.41 ± 0.49	2, 6
Naphthalene	C ₁₀ H ₈	8.144 ± 0.001	51 ± 10	$(1.58 \pm 0.54) \times 10^{-4}$	1.01 ± 0.35	7
Phenanthrene	C ₁₄ H ₁₀	7.891 ± 0.001	56 ± 11	$(1.18 \pm 0.41) \times 10^{-5}$	0.11 ± 0.04	7
Total	40.12 ± 18.05	...

Note.

^a Assuming that the ion signal detected is due solely to the listed isomer.

References. (1) Cool et al. 2005; (2) Kanno & Tonokura 2007; (3) Person 1965; (4) Rennie et al. 1998; (5) Yoshino et al. 1973; (6) Zhou et al. 2009b; (7) Laboratory 2017.

the vinylacetylene and benzene molecules can be formally observed as consisting of two and three acetylene units, respectively, this agrees with excited acetylene interacting with neighboring acetylene molecules, but diacetylene does not consist directly of an acetylene unit but rather two ethynyl (C₂H) units, and the ethynyl radical was not detected.

PI-ReTOF-MS was also used to determine the yields for diacetylene, vinylacetylene, benzene, phenylacetylene, styrene, naphthalene, and phenanthrene as $(2.66 \pm 0.93) \times 10^{-3}$ molecules eV⁻¹, $(5.47 \pm 2.19) \times 10^{-3}$ molecules eV⁻¹, $(3.72 \pm 1.28) \times 10^{-3}$ molecules eV⁻¹, $(4.66 \pm 1.60) \times 10^{-4}$ molecules eV⁻¹, $(2.74 \pm 0.94) \times 10^{-4}$ molecules eV⁻¹, $(1.58 \pm 0.54) \times 10^{-4}$ molecules eV⁻¹, and $(1.18 \pm 0.41) \times 10^{-5}$, respectively (Table 6). Also, the FTIR molecular yields for diacetylene, vinylacetylene, and benzene can then be compared to those determined via PI-ReTOF-MS, and there is good agreement between these different methods. The ethylene yield was not determined from SPI-ReTOF-MS data, as the 10.49 eV photoionization energy used is at the threshold of ethylene photoionization (10.51 eV) (Lias et al.). The sensitive PI-ReTOF-MS techniques detected many more products than FTIR analysis, including phenylacetylene, styrene, naphthalene, and phenanthrene, which were produced in a relative ratio of $314 \pm 126:39 \pm 16:23 \pm 9:13 \pm 5:1 \pm 0.4$ (Benzene:Phenylacetylene:Styrene:Naphthalene:Phenanthrene), which clearly shows a decrease in abundance compared to benzene and supports the previous discussion that benzene is a building block for these more complex aromatic hydrocarbons. Interestingly, with the addition of benzene rings, the yields drop from benzene

via naphthalene to phenanthrene by approximately one order of magnitude each, which suggests a PAH growth mechanism involving a stepwise process in the irradiated acetylene ices (Abplanalp et al. 2019). The FTIR-detected products account for $70.57\% \pm 29.40\%$ of the destroyed acetylene, while the REMPI-detected products account for $40.12\% \pm 18.05\%$ of the destroyed acetylene, showing that the products detected are the major molecules produced.

5. Astrophysical Implications

In the ISM, low-temperature ices consisting of water (H₂O), ammonia (NH₃), carbon dioxide (CO₂), carbon monoxide (CO), formaldehyde (H₂CO), methanol (CH₃OH), and methane (CH₄) have been detected (Boogert et al. 2015). Furthermore, hydrocarbon ices containing methane, ethane, and/or acetylene have been probed on several objects, including Titan (Griffith et al. 2006), Pluto (Holler et al. 2014), Makemake (Brown et al. 2015), and Quaoar (Dalle Ore et al. 2009). Although no pure acetylene ices have been detected yet, the processing of laboratory methane ices results in the formation of the C2 hydrocarbons acetylene, ethylene, and ethane (Bennett et al. 2006; Abplanalp et al. 2018c). These C1 and C2 hydrocarbons have been shown to be instrumental in the buildup of important aromatic molecules from benzene (Zhou et al. 2010) up to PAHs (Kaiser & Roessler 1997; Jones & Kaiser 2013; Abplanalp et al. 2019). Therefore, the examination and understanding of the chemistry that is taking place within these small hydrocarbons are necessary to elucidate the

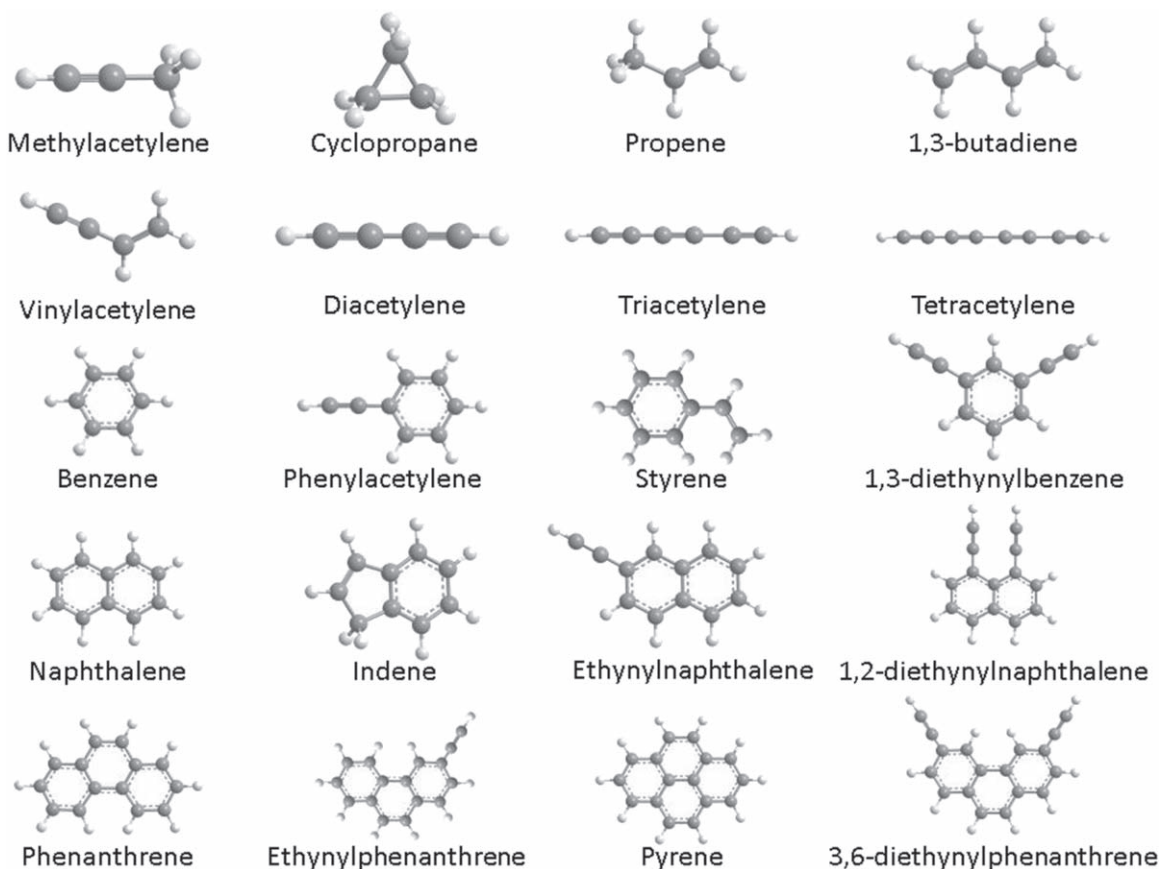


Figure 15. Several possible complex hydrocarbon molecules corresponding to ion signals detected subliming, via PI-ReTOF-MS, from irradiated acetylene ice.

formation routes of the hydrocarbons present in both interstellar and planetary ices.

Here, the irradiation of acetylene ice resulted in the detection of five molecules after FTIR analysis: ethane (C_2H_6/C_2D_6), ethylene (C_2H_4/C_2D_4), diacetylene (C_4H_2/C_4D_2), vinylacetylene (C_4H_4/C_4D_4), and benzene (C_6H_6/C_6D_6). The sensitive PI-ReTOF-MS study using TPD, simulating the transition of a cold molecular cloud into a star-forming region or comets approaching the Sun, was able to detect a much more complex array of product groups: C_nH_{2n+2} ($n = 4, 6-16$), C_nH_{2n} ($n = 2, 3, 6, 8-16$), C_nH_{2n-2} ($n = 3, 4, 6, 8, 10-15$), C_nH_{2n-4} ($n = 4-8, 10-14$), C_nH_{2n-6} ($n = 4-10, 12-16$), C_nH_{2n-8} ($n = 6-10, 12, 14-17$), C_nH_{2n-10} ($n = 6-12, 14-17$), C_nH_{2n-12} ($n = 8-14$), C_nH_{2n-14} ($n = 8-16$), and C_nH_{2n-16} ($n = 10-16$). The production of these hydrocarbon groups of varying degrees of hydrogenation displays that very complex chemistry occurs even in simple starting materials such as acetylene. There are many individual molecules represented by these groups that hold important astrophysical relevance.

The C_nH_{2n} and C_nH_{2n-2} hydrocarbon groups detected here have also been detected in the ISM via the propylene molecule (CH_2CHCH_3) toward TMC-1 (Marcelino et al. 2007; Lin et al. 2013; Rawlings et al. 2013) and methylacetylene (CH_3C_2H) toward Sgr B2, PKS 1830-211, L1544, and tentatively in NCG 4418 (Belloche et al. 2013; Muller et al. 2014; Vastel et al. 2014; Costagliola et al. 2015). The propylene molecule is an important starting material for PAH precursors such as the methylpropargyl radical (C_4H_5) (Kaiser et al. 1997), as well as 1- and 3-vinylpropargyl (Dangi et al. 2013). Although only methylacetylene, but not its isomer allene, has been detected in

the ISM, both isomers participate in the formation of PAHs (Yang et al. 2015b) such as indene (C_9H_8) via the bimolecular reaction with the phenyl radical (C_6H_5) (Parker et al. 2011, 2015b; Zhang et al. 2011a).

Although vinylacetylene, a member of the C_nH_{2n-4} group detected here, has not been detected in the ISM, it has been observed to react with a phenyl radical in the gas phase to form the simplest PAH naphthalene ($C_{10}H_8$) containing two fused benzene rings (Parker et al. 2012). Interestingly, the C_nH_{2n-6} , C_nH_{2n-10} , and C_nH_{2n-14} hydrocarbon groups have all been detected in the ISM in CRL 618 via the polyynic molecules diacetylene, triacetylene, and tetracetylene, respectively (Cernicharo et al. 2001; Kaiser et al. 2010b). CRL 618 was also the location of a detection of the aromatic hydrocarbon benzene (Cernicharo et al. 2001). Jones et al. (2011) proved benzene synthesis in the gas phase via the reaction of the ethynyl radical and 1, 3-butadiene. Several reactions that benzene can then undergo have also been studied in the gas phase with phenyl radicals (C_6H_5) (Zhang et al. 2008), tricarbon molecules (Gu et al. 2007a), dicarbon (Gu et al. 2007b), and carbon atoms (Bettinger et al. 2000; Kaiser et al. 2003) producing diphenyl ($C_6H_5C_6H_5$), phenyltricarbon (C_6H_5CCC), phenylethynyl radical (C_6H_5CC), and 1, 2-didehydrocycloheptatrienyl radical (C_7H_5), respectively. Also, other astronomically relevant molecules, closely related to these experiments through their acetylene subunits, detected in the ISM include methyl diacetylene and methyltriacetylene toward TMC-1 (Loren et al. 1984; MacLeod et al. 1984; Walmsley et al. 1984; Remijan et al. 2006). From the C_nH_{2n-8} group detected here the ortho-benzyne molecule

($\text{o-C}_6\text{H}_4$) was an observed product from the gas-phase reaction of the ethynyl radical with vinylacetylene (Zhang et al. 2011b). Also in this hydrocarbon group ($\text{C}_n\text{H}_{2n-8}$) is the styrene molecule, which was reacted with ethynyl radicals (C_2H) to investigate PAH growth mechanisms. This brief list of detected molecules in the ISM, or molecules related to the production of detected ISM molecules, shows that the products of acetylene irradiation are common interstellar molecules and that acetylene may be a key component to interstellar chemistry. These products can be synthesized on interstellar grains and then can sublime into the gas phase to further react as the molecular cloud transitions to a star-forming region and warms the icy grains just as simulated in the present experiments.

The results presented here represent a necessary starting point to fully understand the complete network of hydrocarbon chemical reactions available during the chemical evolution of binary or even more complex ices. Although laboratory astrochemistry experiments studying complex ice mixtures have been performed for several decades to understand the chemical evolution in the ISM, as well as within our solar system, the implementation of new sensitive techniques has provided information on previously studied systems that were thought to be exhausted. Furthermore, the use of these new techniques, coupled with traditional methods, has led to such a diverse assortment of products detected that complex products are very difficult to decipher even using relatively simple binary ices (Khare et al. 1989; Hudson & Moore 1997, 1999, 2003; Moore & Hudson 1998; Robert Wu et al. 2002; Zhou et al. 2008; Hudson & Loeffler 2013; Carlson et al. 2016; Hitomi et al. 2017; Keane 2017). Therefore, a systematic study of simple analog ices is needed to further develop the understanding of formation pathways present in these ices before attempting to investigate complex model interstellar ices. This acetylene ice may be viewed as a model ice, but without an understanding of the chemical complexity possible via each ice constituent of a more complex model ice, the understanding will be lacking important chemical details. Here, a bottom-up approach to exploring the extraterrestrial hydrocarbon chemistry, which can also be applied to the chemical pathways present in our solar system on different objects, is a first step to the understanding of the chemical pathways needed to produce complex molecules in astrophysical environments such as PAH precursors and PAHs (Figure 15). The very recent detection of the benzene derivative benzonitrile ($\text{c-C}_6\text{H}_5\text{CN}$) (McGuire et al. 2018) formed via the neutral-neutral reaction of the cyano radical (CN) with benzene (Balucani et al. 1999, 2000a; Bennett et al. 2010) shows how important understanding the formation and further chemical evolution of aromatic molecules such as benzene is to the astrochemistry community.

The authors acknowledge support from the US National Science Foundation (AST-1800975) to carry out the experiments. Furthermore, we thank the W. M. Keck Foundation for financing the experimental setup.

ORCID iDs

Ralf I. Kaiser  <https://orcid.org/0000-0002-7233-7206>

References

- Abplanalp, M. J., Borsuk, A., Jones, B. M., & Kaiser, R. I. 2015, *ApJ*, **814**, 45
- Abplanalp, M. J., Förstel, M., & Kaiser, R. I. 2016a, *CPL*, **644**, 79
- Abplanalp, M. J., Frigge, R., & Kaiser, R. I. 2019, *SciA*, **5**, eaaw5841
- Abplanalp, M. J., Góbi, S., Bergantini, A., Turner, A. M., & Kaiser, R. I. 2018a, *ChemPhysChem*, **19**, 556
- Abplanalp, M. J., Góbi, S., & Kaiser, R. I. 2018b, *PCCP*, **21**, 5378
- Abplanalp, M. J., Gozem, S., Krylov, A. I., et al. 2016b, *PNAS*, **113**, 7727
- Abplanalp, M. J., Jones, B. M., & Kaiser, R. I. 2018c, *PCCP*, **20**, 5435
- Abplanalp, M. J., & Kaiser, R. I. 2016, *ApJ*, **827**, 132
- Abplanalp, M. J., & Kaiser, R. I. 2017, *ApJ*, **836**, 195
- Adam, T. W., Clairrotte, M., Streibel, T., et al. 2012, *Analytical and Bioanalytical Chemistry*, **404**, 273
- Allamandola, L., Tielens, A., & Barker, J. 1989, *ApJS*, **71**, 733
- Allamandola, L. J., Hudgins, D. M., & Sandford, S. A. 1999, *ApJL*, **511**, L115
- Balucani, N., Asvany, O., Chang, A. H. H., et al. 1999, *JChPh*, **111**, 7457
- Balucani, N., Asvany, O., Huang, L. C. L., et al. 2000a, *ApJ*, **545**, 892
- Balucani, N., Asvany, O., Osamura, Y., et al. 2000b, *P&SS*, **48**, 447
- Bast, J. E., Lahuis, F., van Dishoeck, E. F., & Tielens, A. G. G. M. 2013, *A&A*, **551**, A118
- Bauschlicher, C. W., Langhoff, S. R., Sandford, S. A., & Hudgins, D. M. 1997, *JPCA*, **101**, 2414
- Beegle, L. W., Wdowiak, T. J., Robinson, M. S., et al. 1997, *ApJ*, **487**, 976
- Belloche, A., Müller, H. S., Menten, K. M., Schilke, P., & Comito, C. 2013, *A&A*, **559**, 1
- Bennett, C. J., Brotton, S. J., Jones, B. M., et al. 2013, *AnaCh*, **85**, 5659
- Bennett, C. J., Jamieson, C. S., Osumura, Y., & Kaiser, R. I. 2006, *ApJ*, **653**, 792
- Bennett, C. J., Morales, S. B., Le Picard, S. D., et al. 2010, *PCCP*, **12**, 8737
- Bera, P. P., Peverati, R., Head-Gordon, M., & Lee, T. J. 2015, *PCCP*, **17**, 1859
- Bergantini, A., Abplanalp, M. J., Pokhilkov, P., et al. 2018a, *ApJ*, **860**, 108
- Bergantini, A., Frigge, R., & Kaiser, R. I. 2018b, *ApJ*, **859**, 59
- Bergantini, A., Góbi, S., Abplanalp, M. J., & Kaiser, R. I. 2018c, *ApJ*, **852**, 70
- Bergantini, A., Maksyutenko, P., & Kaiser, R. I. 2017, *ApJ*, **841**, 96
- Bergantini, A., Zhu, C., & Kaiser, R. I. 2018d, *ApJ*, **862**, 140
- Bettinger, H. F., Schleyer, P. v. R., Schaefer, H. F., III, et al. 2000, *JChPh*, **113**, 4250
- Bézar, B., Drossart, P., Encrenaz, T., & Feuchtgruber, H. 2001, *Icar*, **154**, 492
- Boogert, A. C. A., Gerakines, P. A., & Whittet, D. C. B. 2015, *ARAA*, **53**, 541
- Bottger, G. L., & Eggers, D. F., Jr. 1964, *JChPh*, **40**, 2010
- Bouwman, J., de Haas, A. J., & Oomens, J. 2016, *ChCom*, **52**, 2636
- Brooke, T. Y., Tokunaga, A. T., Weaver, H. A., et al. 1996, *Natur*, **383**, 606
- Brown, M. E., Schaller, E. L., & Blake, G. A. 2015, *AJ*, **149**, 105
- Brown, R. H., Soderblom, L. A., Soderblom, J. M., et al. 2008, *Natur*, **454**, 607
- Burgdorf, M., Orton, G., van Cleve, J., Meadows, V., & Houck, J. 2006, *Icar*, **184**, 634
- Callahan, M. P., Gerakines, P. A., Martin, M. G., Peeters, Z., & Hudson, R. L. 2013, *Icar*, **226**, 1201
- Cané, E., Miani, A., Palmieri, P., Tarroni, R., & Trombetti, A. 1997, *AcSpA*, **53**, 1839
- Cané, E., Miani, A., & Trombetti, A. 2007, *JPCA*, **111**, 8218
- Carlson, R. W., Baines, K. H., Anderson, M. S., Filacchione, G., & Simon, A. A. 2016, *Icar*, **274**, 106
- Cataldo, F. 2004, *Tetrahedron*, **60**, 4265
- Cernicharo, J., Heras, A. M., Tielens, A. G. G. M., et al. 2001, *ApJL*, **546**, L123
- Cockett, M. C. R., Ozeki, H., Okuyama, K., & Kimura, K. 1993, *JChPh*, **98**, 7763
- Compagnini, G., D'Urso, L., Puglisi, O., Baratta, G. A., & Strazzulla, G. 2009, *Carbon*, **47**, 1605
- Cool, T. A., Wang, J., Nakajima, K., Taatjes, C. A., & McLroy, A. 2005, *IJMSp*, **247**, 18
- Cordier, D., Barnes, J. W., & Ferreira, A. G. 2013, *Icar*, **226**, 1431
- Cordier, D., Mousis, O., Lunine, J. I., Lavvas, P., & Vuitton, V. 2009, *ApJL*, **707**, L128
- Costagliola, F., Sakamoto, K., Muller, S., et al. 2015, *A&A*, **582**, A91
- Coustonis, A., Achterberg, R. K., Conrath, B. J., et al. 2007, *Icar*, **189**, 35
- Coustonis, A., Salama, A., Schulz, B., et al. 2003, *Icar*, **161**, 383
- Crovisier, J., Bockelée-Morvan, D., Colom, P., et al. 2004, *A&A*, **418**, 1141
- Cunshun, H., Fangtong, Z., Ralf, I. K., et al. 2010, *ApJ*, **714**, 1249
- Cuyllé, S. H., Zhao, D., Strazzulla, G., & Linnartz, H. 2014, *A&A*, **570**, 1
- Dalle Ore, C., Morea Barucci, M. A., Emery, J. P., et al. 2009, *A&A*, **501**, 349
- da Silva, G. 2014, *JPCA*, **118**, 3967
- Dangi, B. B., Maity, S., Kaiser, R. I., & Mebel, A. M. 2013, *JPCA*, **117**, 11783
- Dartois, E., Caro, G. M. M., Deboffle, D., Montagnac, G., & d'Hendecourt, L. 2005, *A&A*, **432**, 895
- Dawes, A., Pascual, N., Hoffmann, S. V., Jones, N. C., & Mason, N. J. 2017, *PCCP*, **19**, 27544
- de la Cruz, A., Ortiz, M., Cabrera, J. A., & Campos, J. 1994, *IJMPDN*, **133**, 39

- Despois, D. 1997, *EM&P*, **79**, 103
- DiSanti, M. A., Bonev, B. P., Gibb, E. L., et al. 2016, *ApJ*, **820**, 34
- Doney, K. D., Zhao, D., Stanton, J. F., & Linnartz, H. 2018, *PCCP*, **20**, 5501
- Drouin, D., Couture, A. R., Joly, D., et al. 2007, *Scanning*, **29**, 92
- Duley, W. W., & Anming, H. 2009, *ApJ*, **698**, 808
- Floyd, G., Prince, R., & Duley, W. 1973, *JRASA*, **67**, 299
- Fonfría, J. P., Cernicharo, J., Richter, M. J., & Lacy, J. H. 2011, *ApJ*, **728**, 43
- Förstel, M., Bergantini, A., Maksyutenko, P., Góbi, S., & Kaiser, R. I. 2017, *ApJ*, **845**, 83
- Förstel, M., Maksyutenko, P., Jones, B. M., et al. 2015, *ChemPhysChem*, **16**, 3139
- Förstel, M., Maksyutenko, P., Jones, B. M., et al. 2016a, *ApJ*, **820**, 117
- Förstel, M., Maksyutenko, P., Jones, B. M., et al. 2016b, *ChCom*, **52**, 741
- Förstel, M., Maksyutenko, P., Mebel, A. M., & Kaiser, R. I. 2016c, *ApJL*, **818**, L30
- Förstel, M., Tsegaw, Y. A., Maksyutenko, P., et al. 2016d, *ChemPhysChem*, **17**, 2726
- Frigge, R., Zhu, C., Turner, A. M., et al. 2018a, *ApJ*, **862**, 84
- Frigge, R., Zhu, C., Turner, A. M., et al. 2018b, *ChCom*, **54**, 10152
- Gelpi, E., & Oró, J. 1970, *IUMIP*, **4**, 323
- Gibb, E. L., Brunt, K. A. V., Brittain, S. D., & Rettig, T. W. 2007, *ApJ*, **660**, 1572
- Gladstone, G. R., Stern, S. A., Ennico, K., et al. 2016, *Sci*, **351**, aad8866
- Góbi, S., Bergantini, A., & Kaiser, R. I. 2016, *ApJ*, **832**, 164
- Góbi, S., Bergantini, A., & Kaiser, R. I. 2017a, *ApJ*, **838**, 84
- Góbi, S., Bergantini, A., Turner, A. M., & Kaiser, R. I. 2017b, *JPCA*, **121**, 3879
- Góbi, S., Crandall, P. B., Maksyutenko, P., Förstel, M., & Kaiser, R. I. 2018, *JPCA*, **122**, 2329
- Góbi, S., Förstel, M., Maksyutenko, P., & Kaiser, R. I. 2017c, *ApJ*, **835**, 241
- Goulay, F., Osborn, D. L., Taatjes, C. A., et al. 2007, *PCCP*, **9**, 4291
- Griffith, C. A., Penteado, P., Rannou, P., et al. 2006, *Sci*, **313**, 1620
- Groner, P., Stolkin, I., & Gunthard, H. H. 1973, *JPhE*, **6**, 122
- Gu, X., Guo, Y., Mebel, A. M., & Kaiser, R. I. 2007a, *CPL*, **449**, 44
- Gu, X., Guo, Y., Zhang, F., Mebel, A. M., & Kaiser, R. I. 2007b, *CPL*, **436**, 7
- Gu, X., Kim, Y. S., Kaiser, R. I., et al. 2009, *PNAS*, **106**, 16078
- Gudipati, M. S., & Yang, R. 2012, *ApJL*, **756**, L24
- Guerlet, S., Fouchet, T., Bézard, B., et al. 2010, *Icar*, **209**, 682
- Hager, J. W., & Wallace, S. C. 1988, *AnaCh*, **60**, 5
- Halasinski, T. M., Salama, F., & Allamandola, L. J. 2005, *ApJ*, **628**, 555
- Hiraoka, K., & Sato, T. 2001, *RaPC*, **60**, 389
- Hiraoka, K., Takayama, T., Euchii, A., Handa, H., & Sato, T. 2000, *ApJ*, **532**, 1029
- Hitomi, K., Hiroshi, H., Thanja, L., et al. 2017, *ApJ*, **837**, 155
- Hollenberg, J. L., & Dows, D. A. 1962, *JChPh*, **37**, 1300
- Holler, B. J., Young, L. A., Grundy, W. M., Olkin, C. B., & Cook, J. C. 2014, *Icar*, **243**, 104
- Hörst, S. M. 2017, *JGRE*, **122**, 432
- Hudgins, D. M., & Sandford, S. A. 1998, *JPCA*, **102**, 329
- Hudgins, D. M., Sandford, S. A., & Allamandola, L. J. 1994, *JPhCh*, **98**, 4243
- Hudson, R., Gerakines, P., & Moore, M. 2014a, *Icar*, **243**, 148
- Hudson, R. L., Ferrante, R. F., & Moore, M. H. 2014b, *Icar*, **228**, 276
- Hudson, R. L., & Loeffler, M. J. 2013, *ApJ*, **773**, 109
- Hudson, R. L., & Moore, M. H. 1997, *Icar*, **126**, 233
- Hudson, R. L., & Moore, M. H. 1999, *Icar*, **140**, 451
- Hudson, R. L., & Moore, M. H. 2003, *ApJL*, **586**, L107
- Jiménez-Redondo, M., Tanarro, I., Peláez, R. J., Díaz-Pérez, L., & Herrero, V. J. 2019, *JPCA*, **123**, 8135
- Jolly, A., & Benilan, Y. 2008, *JQSRAE*, **109**, 963
- Jones, B., Zhang, F., Maksyutenko, P., Mebel, A. M., & Kaiser, R. I. 2010, *JPCA*, **114**, 5256
- Jones, B. M., & Kaiser, R. I. 2013, *JPhChL*, **4**, 1965
- Jones, B. M., Kaiser, R. I., & Strazzulla, G. 2014a, *ApJ*, **781**, 85
- Jones, B. M., Kaiser, R. I., & Strazzulla, G. 2014b, *ApJ*, **788**, 170
- Jones, B. M., Zhang, F., Kaiser, R. I., et al. 2011, *PNAS*, **108**, 452
- Kaiser, R. I., Eich, G., Gabrysch, A., & Roessler, K. 1997a, *ApJ*, **484**, 487
- Kaiser, R. I., Mahfouz, R. M., & Roessler, K. 1992, *NIMPB*, **65**, 468
- Kaiser, R. I., Maity, S., & Jones, B. M. 2014, *PCCP*, **16**, 3399
- Kaiser, R. I., Maity, S., & Jones, B. M. 2015, *Angewandte Chemie International Edition*, **54**, 195
- Kaiser, R. I., & Maksyutenko, P. 2015a, *CPL*, **631**, 59
- Kaiser, R. I., & Maksyutenko, P. 2015b, *JPCP*, **119**, 14653
- Kaiser, R. I., Maksyutenko, P., Ennis, C., et al. 2010a, *FaDi*, **147**, 429
- Kaiser, R. I., & Mebel, A. M. 2012, *Chemical Society Reviews*, **41**, 5490
- Kaiser, R. I., & Roessler, K. 1997, *ApJ*, **475**, 144
- Kaiser, R. I., & Roessler, K. 1998, *ApJ*, **503**, 959
- Kaiser, R. I., Stockton, A. M., Kim, Y. S., Jensen, E. C., & Mathies, R. A. 2013, *ApJ*, **765**, 111
- Kaiser, R. I., Stranges, D., Bevsek, H. M., Lee, Y. T., & Suits, A. G. 1997b, *JChPh*, **106**, 4945
- Kaiser, R. I., Sun, B. J., Lin, H. M., et al. 2010b, *ApJ*, **719**, 1884
- Kaiser, R. I., Vereecken, L., Peeters, J., et al. 2003, *A&A*, **406**, 385
- Kanno, N., & Tonokura, K. 2007, *ApSpe*, **61**, 896
- Keane, T. C. 2017, *OLEB*, **47**, 223
- Khare, B., Thompson, W., Murray, B., et al. 1989, *Icar*, **79**, 350
- Kim, Y. S., Bennett, C. J., Li-Hsieh, C., Brien, K. O., & Kaiser, R. I. 2010, *ApJ*, **711**, 744
- Kim, Y. S., & Kaiser, R. I. 2009, *ApJS*, **181**, 543
- Klimcak, C. M., & Wessel, J. E. 1980, *AnaCh*, **52**, 1233
- Laboratory, N. S. R. 2017, Photonionization Cross Section Database (Version 2.0)
- Lacy, J., Evans, N. J., Achtermann, J., et al. 1989, *ApJL*, **342**, L43
- Lahuis, F., & Van Dishoeck, E. 2000, *A&A*, **355**, 699
- Landera, A., Kaiser, R. I., & Mebel, A. M. 2011, *JChPh*, **134**, 024302
- Lias, S. G., Bartmess, J. E., Liebman, J. F., et al. in NIST Chemistry WebBook, NIST Standard Reference Database Number 69, ed. P. J. Linstrom & W. G. Mallard (Gaithersburg, MD: National Institute of Standards and Technology)
- Lin, Z., Talbi, D., Roueff, E., et al. 2013, *ApJ*, **765**, 80
- Linden, C. F., Zabka, J., Polasek, M., Zymak, I., & Geppert, W. D. 2018, *PCCP*, **20**, 5377
- Lindén, F., Alcaraz, C., Ascenzi, D., et al. 2016, *JPCA*, **120**, 5337
- Loren, R. B., Wooten, A., & Mundy, L. G. 1984, *ApJL*, **286**, L23
- Lorenz, R. D., Wall, S., Radebaugh, J., et al. 2006, *Sci*, **312**, 724
- Lunine, J. I., & Hörst, S. M. 2011, *Rendiconti Lincei*, **22**, 183
- Mackie, C. J., Candian, A., Huang, X., et al. 2018, *PCCP*, **20**, 1189
- MacLeod, J. M., Avery, L. W., & Broten, N. W. 1984, *ApJL*, **282**, L89
- Maity, S., Kaiser, R. I., & Jones, B. M. 2014a, *ApJ*, **789**, 36
- Maity, S., Kaiser, R. I., & Jones, B. M. 2014b, *FaDi*, **168**, 485
- Maity, S., Kaiser, R. I., & Jones, B. M. 2015, *PCCP*, **17**, 3081
- Maksyutenko, P., Förstel, M., Crandall, P., et al. 2016, *CPL*, **658**, 20
- Maksyutenko, P., Muzangwa, L. G., Jones, B. M., & Kaiser, R. I. 2015, *PCCP*, **17**, 7514
- Mallocci, G., Joblin, C., & Mulas, G. 2007, *A&A*, **462**, 627
- Mallocci, G., Mulas, G., & Joblin, C. 2004, *A&A*, **426**, 105
- Marcelino, N., Cernicharo, J., Agúndez, M., et al. 2007, *ApJL*, **665**, L127
- McGuire, B. A., Burkhardt, A. M., Kalenskii, S., et al. 2018, *Sci*, **359**, 202
- McMullan, R. K., Kvick, A., & Popelier, P. 1992, *Acta Crystallographica Section B*, **48**, 726
- McMurtry, B. M., Saito, S. E. J., Turner, A. M., Chakravarty, H. K., & Kaiser, R. I. 2016, *ApJ*, **831**, 174
- Mebel, A. M., Kislov, V. V., & Kaiser, R. I. 2008, *JChS*, **130**, 13618
- Mejía, C. F., de Barros, A. L. F., Bordalo, V., et al. 2013, *MNRAS*, **433**, 2368
- Moore, M. H., & Hudson, R. L. 1998, *Icar*, **135**, 518
- Moses, J. I., Bézard, B., Lellouch, E., et al. 2000, *Icar*, **143**, 244
- Mulas, G., Mallocci, G., Joblin, C., & Toubanc, D. 2006, *A&A*, **460**, 93
- Muller, S., Combes, F., Guélin, M., et al. 2014, *A&A*, **566**, A112
- Mumma, M. J., DiSanti, M. A., Magee-Sauer, K., et al. 2005, *Sci*, **310**, 270
- Ota, N. 2017, arXiv:1704.06197
- Palmer, M. Y., Cordiner, M. A., Nixon, C. A., et al. 2017, *SciA*, **3**, e1700022
- Parker, D. S. N., Dangi, B. B., Kaiser, R. I., et al. 2014a, *JPCA*, **118**, 2709
- Parker, D. S. N., Dangi, B. B., Kaiser, R. I., et al. 2014b, *JPCA*, **118**, 12111
- Parker, D. S. N., Kaiser, R. I., Bandyopadhyay, B., et al. 2015a, *Angewandte Chemie International Edition*, **54**, 5421
- Parker, D. S. N., Kaiser, R. I., Kostko, O., & Ahmed, M. 2015b, *ChemPhysChem*, **16**, 2091
- Parker, D. S. N., Zhang, F., Kaiser, R. I., Kislov, V. V., & Mebel, A. M. 2011, *Chemistry—An Asian Journal*, **6**, 3035
- Parker, D. S. N., Zhang, F., Kim, Y. S., et al. 2012, *PNAS*, **109**, 53
- Pathak, A., Buragohain, M., Hammonds, M., & Sarre, P. J. 2014, *IAU Proc.* **297**, The Diffuse Interstellar Band (Cambridge: Cambridge Univ. Press), 349
- Pauzat, F., & Ellinger, Y. 2001, *MNRAS*, **324**, 355
- Pauzat, F., Talbi, D., & Ellinger, Y. 1995, *A&A*, **293**, 263
- Person, J. C. 1965, *JChPh*, **43**, 2553
- Puglisi, O., Compagnini, G., D'Urso, L., et al. 2014, *NIMPB*, **326**, 2
- Rawlings, J. M. C., Williams, D. A., Viti, S., & Cecchi-Pestellini, C. 2013, *MNRAS*, **436**, L59
- Remijan, A. J., Hollis, J. M., Snyder, L. E., Jewell, P. R., & Lovas, F. J. 2006, *ApJL*, **643**, L37
- Rennie, E., Johnson, C., Parker, J., et al. 1998, *CP*, **229**, 107
- Ridgway, S. 1974, *ApJL*, **187**, L41

- Ridgway, S. T., Hall, D. N. B., Kleinmann, S. G., Weinberger, D. A., & Wojslaw, R. S. 1976, *Natur*, **264**, 345
- Robert Wu, C. Y., Judge, D. L., Cheng, B.-M., et al. 2002, *Icar*, **156**, 456
- Ryazantsev, S. V., Zaslomov, P. V., & Feldman, V. I. 2018, *RaPC*, **151**, 253
- Sandford, S. A., Bernstein, M. P., & Allamandola, L. J. 2004, *ApJ*, **607**, 346
- Sekiguchi, T., Watanabe, J., Fukushima, H., Yamamoto, T., & Yamamoto, N. 1997, *EM&P*, **78**, 143
- Sephton, M. A., Pillinger, C. T., & Gilmour, I. 2001, *PreR*, **106**, 47
- Singh, S., McCord, T. B., Combe, J. P., et al. 2016, *ApJ*, **828**, 55
- Sivaraman, B., Mukherjee, R., Subramanian, K. P., & Banerjee, S. B. 2015, *ApJ*, **798**, 72
- Sonnentrucker, P., González-Alfonso, E., & Neufeld, D. A. 2007, *ApJL*, **671**, L37
- Stahl, F., Schleyer, P. v. R., Schaefer, H. F., III, & Kaiser, R. I. 2002, *P&SS*, **50**, 685
- Stephens, K. M., & Bauer, S. H. 1994, *AcSpA*, **50**, 741
- Stofan, E. R., Elachi, C., Lunine, J. I., et al. 2007, *Natur*, **445**, 61
- Strazzulla, G., Baratta, G. A., Domingo, M., & Satorre, M. A. 2002, *NIMPB*, **191**, 714
- Sun, Y.-L., Huang, W.-J., & Lee, S.-H. 2015, *JPhChL*, **6**, 4117
- Swenson, O. F., & Gillispie, G. D. 1996, *Proc. SPIE*, **2835**, 144
- Tarczay, G., Förstel, M., Góbi, S., Maksyutenko, P., & Kaiser, R. I. 2017, *ChemPhysChem*, **18**, 882
- Tarczay, G., Förstel, M., Maksyutenko, P., & Kaiser, R. I. 2016, *InCh*, **55**, 8776
- Thapa, J., Spencer, M., Akhmedov, N. G., & Goulay, F. 2015, *JPhChL*, **6**, 4997
- Thomas, A. M., Lucas, M., Yang, T., et al. 2017, *ChemPhysChem*, **18**, 1971
- Tian, M., Liu, B. S., Hammonds, M., et al. 2012, *PCCP*, **14**, 6603
- Tørneng, E., Nielsen, C. J., Klæboe, P., Hopf, H., & Priebe, H. 1980, *AcSpA*, **36**, 975
- Tsegaw, Y. A., Góbi, S., Förstel, M., et al. 2017, *JPCA*, **121**, 7477
- Turner, A. M., Abplanalp, M. J., Chen, S. Y., et al. 2015, *PCCP*, **17**, 27281
- Turner, A. M., Abplanalp, M. J., & Kaiser, R. I. 2016, *ApJ*, **819**, 97
- Turner, A. M., Bergantini, A., Abplanalp, M. J., et al. 2018, *NatCo*, **9**, 3851
- Tzeng, W. B., Narayanan, K., & Lin, J. L. 1999, *ApSpe*, **53**, 731
- Vakhtin, A. B., Heard, D. E., Smith, I. W. M., & Leone, S. R. 2001, *CPL*, **344**, 317
- van Loon, J. T., Marshall, J. R., Cohen, M., et al. 2006, *A&A*, **447**, 971
- van Nes, G. J. H. 1978, PhD thesis, Univ. Groningen
- Vastel, C., Ceccarelli, C., Lefloch, B., & Bachiller, R. 2014, *ApJL*, **795**, L2
- Ventura, E., Dallos, M., & Lischka, H. 2003, *JChPh*, **118**, 1702
- Vuitton, V., Yelle, R. V., & Cui, J. 2008, *JGRE*, **113**, E05007
- Vuitton, V., Yelle, R. V., Lavvas, P., & Klippenstein, S. J. 2012, *ApJ*, **744**, 11
- Walmsley, C. M., Jewell, P. R., Snyder, L. E., & Winnewisser, G. 1984, *A&A*, **134**, L11
- Wilson, E. H., & Atreya, S. K. 2009, *JPCA*, **113**, 11221
- Wong, M. L., Fan, S., Gao, P., et al. 2017, *Icar*, **287**, 110
- Woon, D. E., & Park, J.-Y. 2009, *Icar*, **202**, 642
- Wu, Y.-J., & Cheng, B.-M. 2008, *CPL*, **461**, 53
- Wu, Y.-J., Chuang, S.-J., Chen, S.-C., & Huang, T.-P. 2014, *ApJS*, **212**, 7
- Xibin Gu, F. Z., Guo, Y., & Kaiser, R. I. 2007, *Angewandte Chemie International Edition in English*, **46**, 6866
- Yamada, H., & Saheki, M. 1983, *Bulletin of the Chemical Society of Japan*, **56**, 35
- Yang, T., Kaiser, R. I., Troy, T. P., et al. 2017, *Angewandte Chemie International Edition*, **56**, 4515
- Yang, T., Muzangwa, L., Kaiser, R. I., Jamal, A., & Morokuma, K. 2015a, *PCCP*, **17**, 21564
- Yang, T., Parker, D. S. N., Dangi, B. B., Kaiser, R. I., & Mebel, A. M. 2015b, *PCCP*, **17**, 10510
- Yang, X. J., Glaser, R., Li, A., & Zhong, J. X. 2013, *ApJ*, **776**, 110
- Yoshino, M., Takeuchi, J., & Suzuki, H. 1973, *JPSJ*, **34**, 1039
- Zarnecki, J. C., Leese, M. R., Hathi, B., et al. 2005, *Natur*, **438**, 792
- Zhang, F., Gu, X., Guo, Y., & Kaiser, R. I. 2007, *JOC*, **72**, 7597
- Zhang, F., Gu, X., & Kaiser, R. I. 2008, *JChPh*, **128**, 084315
- Zhang, F., Jones, B., Maksyutenko, P., et al. 2010, *JChS*, **132**, 2672
- Zhang, F., Kaiser, R. I., Kislov, V. V., et al. 2011a, *JPhChL*, **2**, 1731
- Zhang, F., Kim, S., & Kaiser, R. I. 2009a, *PCCP*, **11**, 4707
- Zhang, F., Kim, S., Kaiser, R. I., & Mebel, A. M. 2009b, *JPCA*, **113**, 1210
- Zhang, F., Kim, Y. S., Kaiser, R. I., Krishtal, S. P., & Mebel, A. M. 2009c, *JPCA*, **113**, 11167
- Zhang, F., Parker, D., Kim, S., Kaiser, R. I., & Mebel, A. M. 2011b, *ApJ*, **728**, 141
- Zhang, X., & Sander, S. P. 2017, *CPL*, **688**, 47
- Zheng, W., Jewitt, D., & Kaiser, R. I. 2006, *ApJ*, **648**, 753
- Zhou, L., Kaiser, R. I., Gao, L. G., et al. 2008, *ApJ*, **686**, 1493
- Zhou, L., Kaiser, R. I., & Tokunaga, A. T. 2009a, *P&SS*, **57**, 830
- Zhou, L., Maity, S., Abplanalp, M., Turner, A., & Kaiser, R. I. 2014, *ApJ*, **790**, 38
- Zhou, L., Zheng, W., Kaiser, R. I., et al. 2010, *ApJ*, **718**, 1243
- Zhou, Z., Xie, M., Wang, Z., & Qi, F. 2009b, *RCMS*, **23**, 3994
- Zhu, C., Frigge, R., Turner, A. M., et al. 2018, *ChCom*, **54**, 5716